



# RESEARCH MEMORANDUM

WIND-TUNNEL INVESTIGATION AT LOW SPEED OF A WING

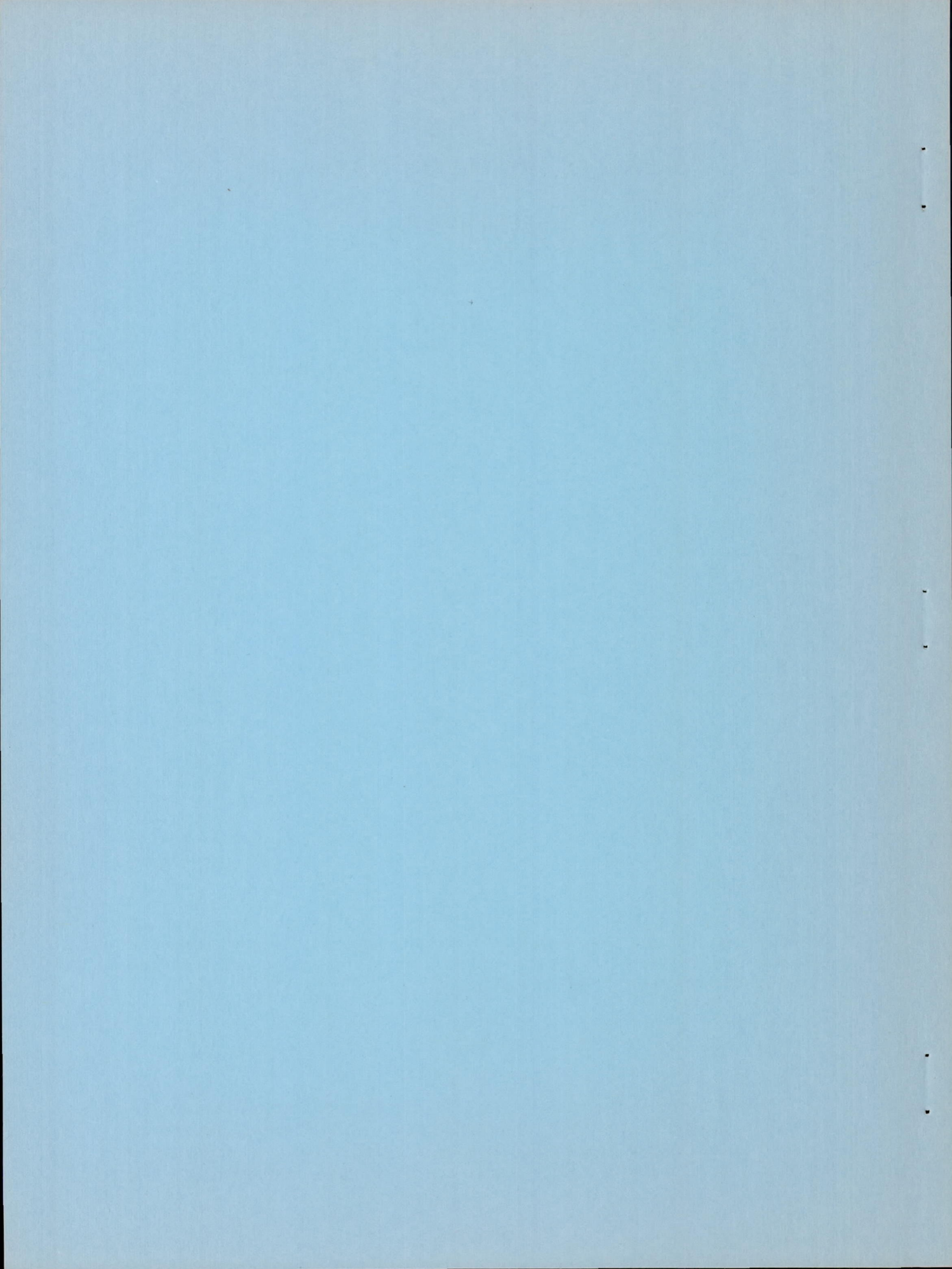
SWEPT BACK  $63^{\circ}$  AND TWISTED AND CAMBERED FOR  
A UNIFORM LOAD AT A LIFT COEFFICIENT OF 0.5

By James A. Weiberg and Hubert C. Carel

Ames Aeronautical Laboratory  
Moffett Field, Calif.

NATIONAL ADVISORY COMMITTEE  
FOR AERONAUTICS  
WASHINGTON

May 9, 1950  
Declassified May 8, 1957



NATIONAL ADVISORY COMMITTEE FOR AERONAUTICS

RESEARCH MEMORANDUM

WIND-TUNNEL INVESTIGATION AT LOW SPEED OF A WING

SWEPT BACK  $63^{\circ}$  AND TWISTED AND CAMBERED FOR

A UNIFORM LOAD AT A LIFT COEFFICIENT OF 0.5

By James A. Weiberg and Hubert C. Carel

SUMMARY

Tests were made to determine the low-speed longitudinal-stability characteristics and the spanwise distribution of load of a semispan model of a wing with the leading edge swept back  $63^{\circ}$ , with an aspect ratio of 3.5, and with a large amount of twist and camber. Tests were also made of the wing with a fuselage, with upper-surface fences, and with leading- and trailing-edge flaps.

Comparisons with the results of tests of a semispan model of an untwisted and uncambered wing of identical plan form showed that the stability characteristics were not improved by the twist and camber. For both the twisted and the untwisted wing, large variations in longitudinal stability occurred with increasing lift coefficient. The variations of longitudinal stability were attributed principally to spanwise boundary-layer flow and separation. Above a lift coefficient of 0.3 the twisted and cambered wing had a higher lift-drag ratio than the untwisted wing. The addition of flaps and upper-surface fences to the wing delayed the initial occurrence of separation and the attendant aerodynamic-center travel to higher lift coefficients.

Within the angle-of-attack range in which lift was not appreciably affected by spanwise boundary-layer flow or separation, good agreement was obtained between the measured span load distribution and that computed by the methods of Weissinger.

INTRODUCTION

Highly swept wings with relatively high aspect ratios designed for efficient flight at moderate supersonic Mach numbers have undesirable lift and stability characteristics at low speeds (i.e., at moderate to high lift coefficients). This fault has been shown in references 1 and 2

from the results of tests of an untwisted and uncambered wing with the leading edge swept back  $63^\circ$ . For this wing, the combined effects of spanwise flow in the boundary layer and flow separation altered the spanwise distribution of load which, because of the large sweep, resulted in variations of the position of the aerodynamic center with lift coefficient. In reference 3, it was reasoned that these undesirable characteristics of swept wings might be alleviated by the use of twist and camber. To determine experimentally if by these means the stability characteristics of a wing swept back  $63^\circ$  could be improved, an investigation was made in one of the Ames 7- by 10-foot wind tunnels of a semi-span model twisted and cambered to give an approximately uniform lift distribution at a lift coefficient of 0.5 and at a Mach number of 1.4. The longitudinal characteristics of this twisted and cambered wing, as shown by force and pressure-distribution measurements, are presented herein. Also presented are the results of tests of the wing with a fuselage and with fences and leading- and trailing-edge flaps.

#### NOTATION AND CORRECTIONS

All data are presented as NACA coefficients corrected for tunnel-wall effects. Forces and moments are those for the semispan model and are referred to the wind axis and to the moment center shown in figure 1. Coefficients and symbols used are defined as follows:

A aspect ratio  $\left(\frac{b^2}{S}\right)$

b span of complete wing perpendicular to the plane of symmetry (twice span of semispan wing), feet

c' wing chord (fig. 2), feet

c projection of wing chord in wing reference plane ( $c' \cos \epsilon$ , fig. 2), feet

$\bar{c}$  mean aerodynamic chord  $\left(\frac{\int_0^{b/2} c^2 dy}{\int_0^{b/2} c dy}\right)$ , feet

$c_{av}$  average chord  $\left(\frac{S}{b}\right)$ , feet

$c_D$  drag coefficient  $\left[\frac{\text{drag}}{q(S/2)}\right]$

$C_L$  lift coefficient  $\left[ \frac{\text{lift}}{q(S/2)} \right]$

$c_l$  section lift coefficient

$C_{L\alpha}$  rate of change of wing lift coefficient with angle of attack  
 $\left( \frac{dC_L}{d\alpha} \right)$

$c_{l\alpha}$  rate of change of section lift coefficient with wing angle of attack  
 $\left( \frac{dc_l}{d\alpha} \right)$

$C_m$  pitching-moment coefficient  $\left[ \frac{\text{pitching moment}}{qc \cdot (S/2)} \right]$

L/D lift-drag ratio

P pressure coefficient  $\left( \frac{p_l - p}{q} \right)$

p free-stream static pressure, pounds per square foot

$p_l$  local static pressure, pounds per square foot

q dynamic pressure, pounds per square foot

R Reynolds number  $\left( \frac{Vc}{\nu} \right)$

S area of complete wing (twice area of semispan model), square feet

x distance measured parallel to X axis (fig. 2), feet

y distance measured perpendicular to plane of symmetry, feet

$y_{c_{\max}}$  maximum camber (fig. 2), percent chord

$\alpha$  angle of attack of wing reference plane,<sup>1</sup> degrees

$\epsilon$  angle of twist (fig. 2), degrees

$\nu$  kinematic viscosity, feet squared per second

---

<sup>1</sup>The wing reference plane contains the wing leading edge and the X and Y axes (fig. 2).

Tunnel-wall corrections were applied to the angle of attack and to the lift and pitching-moment coefficients using methods similar to those of references 4 and 5. The corrections were applied as follows:

$$C_L = 0.991 C_{L_u}$$

$$\alpha = \alpha_u + \Delta\alpha_T$$

$$C_m = C_{m_u} + \Delta C_{m_T}$$

$$C_D = C_{D_u} + \Delta C_{D_T}$$

where

$$\Delta\alpha_T = 1.358 \left( C_{L_u} \right)_{w+f} + 0.190 \left( C_{L_u} \right)_w$$

$$\Delta C_{m_T} = 0.0010 C_{L_u}$$

$$\Delta C_{D_T} = 0.0319 C_{L_u}^2$$

and the subscripts signify

u uncorrected

w wing

f flap

No corrections were applied to the data for possible effects of interference between the model and the tunnel floor or of leakage through the gap between the tunnel floor and the extension of the base of the model where it passed through the floor. However, it was believed that the effects of this interference and leakage on the aerodynamic characteristics of the model were negligible.

At a dynamic pressure of 40 pounds per square foot (corresponding to the maximum test Reynolds number of 3.7 million) and with a lift coefficient of 1.0, the tip of the wing deflected 3 inches and twisted less than  $0.3^\circ$  with respect to its no-load position. Data presented in reference 6 from tests of an untwisted and uncambered wing of the same plan form indicated that only small effects on the aerodynamic characteristics of the wing were produced by deflections of the wing under load. Consequently, no corrections have been applied to the data of the present tests for the effects of model distortion.

## MODEL DESCRIPTION

The wing tested was a semispan model with  $63^\circ$  sweepback of the leading edge, an aspect ratio of 3.5, and a taper ratio of 0.25 (ratio of tip chord to root chord). Dimensions of the wing are shown in figure 1 and table I. The wing was constructed of laminated mahogany and is shown mounted in the wind tunnel in figure 3. The model was mounted with the tunnel floor as a reflection plane; that is, the plane of symmetry of the wing was coincident with the floor of the tunnel. A gap of 1/8 to 1/4 inch existed between the tunnel floor and the extension of the base of the model which passed through the floor to support the model (fig. 3(a)).

The twist and camber of the wing were designed by methods similar to those of reference 7 to give an approximately uniform lift distribution at a lift coefficient of 0.5 and a Mach number of 1.4. To avoid the extreme twist at the root, indicated by the theory of reference 7, the twist and camber of the wing from the fuselage juncture (0.13 semispan) to the root were altered to give the variations shown in figure 4. The twist shown in figure 4 is referred to the wing reference plane. The leading edge of the wing was straight. The thickness distribution of sections in planes perpendicular to the wing leading edge was the NACA 0010 section. The wing was equipped with pressure orifices on sections parallel to the plane of symmetry at 0.200, 0.383, 0.707, and 0.924 semispan.

The fuselage tested on the wing is shown in figures 1 and 3(b). Dimensions of the fuselage are given in figure 1 and in tables I and II. The flaps and the fences tested on the model are shown in figures 3(c), 3(d), 3(e), and 5.

## RESULTS AND DISCUSSION

## Force Measurements

Varying the Reynolds number within the limited range from 2.3 to 3.7 million<sup>2</sup> (based on  $\bar{c}$ ) caused only the small effects on the lift and pitching-moment characteristics of the wing and wing with fuselage shown in figure 6. The results of tests of a wing of similar plan form but not cambered or twisted (reference 6) indicated only small changes in the stability characteristics with an increase of Reynolds number from 4 to 10 million. The remainder of the data presented herein were obtained at a Reynolds number of 3.7 million (1.3 million based on the tip chord) corresponding to a Mach number of 0.16.

---

<sup>2</sup>The corresponding variation of Mach number was from 0.10 to 0.16.

The principal effects of the addition of the fuselage to the wing (fig. 7) were an increase of the angle of attack for zero lift of  $2.5^\circ$  (from  $-6^\circ$  to  $-3.5^\circ$ ), an increase of the lift-curve slope of 0.005 (measured at zero lift) and a decrease of the pitching-moment coefficient at zero lift from 0.08 to 0.02 with no marked change in static longitudinal stability ( $dc_m/dc_L$ ).

The data in figure 7 show that the position of the aerodynamic center as indicated by the slopes of the pitching-moment curves ( $dc_m/dc_L$ ) varied considerably with lift coefficient. A comparison of the characteristics of the wing used in the present investigation with the characteristics of an untwisted and uncambered wing of the same plan form is shown in figure 8. The data in figure 8 for the flat (untwisted and uncambered) wing are from tests of a semispan  $63^\circ$  swept-back wing<sup>3</sup> at a Reynolds number of 4.2 million reported in reference 2. This comparison indicates that the twist and camber provided no improvement in the stability characteristics of the  $63^\circ$  swept wing.

In reference 1, the stability variations of the untwisted wing were attributed principally to spanwise boundary-layer flow and to flow separation near the tip. This spanwise boundary-layer flow and flow separation altered the load distribution and, because of the large sweep, varied the location of the aerodynamic center. The aerodynamic-center variation of the twisted and cambered wing will be discussed later in connection with the results of pressure-distribution measurements.

A comparison of the drag characteristics of the flat wing and the twisted wing is shown in figure 9. The minimum drag coefficient of the twisted wing was greater and occurred at a higher lift coefficient than for the flat wing. A comparison of the maximum lift-drag ratios obtained from figure 9 for the twisted and the flat wings is shown in the following table:

Parameter	Wing		Wing with fuselage	
	Flat	Twisted	Flat	Twisted
$(L/D)_{max}$	17.0	14.5	11.8	13.5
$C_L$ for $(L/D)_{max}$	.17	.33	.28	.30

<sup>3</sup>The wing of reference 2 besides having no twist or camber differed from the wing of the present investigation in that the sections parallel to the root chord were the NACA 64A006.

It may be noted in figure 9(a) that above a lift coefficient of 0.3 the twisted wing had the higher lift-drag ratio. Thus, the twisted and cambered wing would provide a lower rate of descent for an airplane in a landing approach with power off than would the flat wing.

Numerous investigations (e.g., references 8 and 9) have shown that the stability characteristics of highly swept wings can be altered by the use of fences and leading- and trailing-edge flaps. Consequently, flaps and fences were tested on the twisted and cambered wing. These flaps and fences (fig. 5) were not necessarily of optimum design but were used primarily to determine if the stability characteristics of this wing could be improved at moderate to high lift coefficients.

The effect on lift and pitching moment of decreasing the spanwise boundary-layer flow by the use of fences at several span stations on the upper surface of the wing with and without a leading-edge flap is shown in figure 10. Fences reduced the instability of the wing without flaps (fig. 10(a)) within the lift-coefficient range from 0.4 to 0.55 with little change in stability at other positive lift coefficients. With a 0.45-span leading-edge flap, the wing, with either single or combinations of fences, was stable to a lift coefficient of at least 0.75 (fig. 10(b)).

As indicated in figure 11, a slightly greater improvement in the stability of the wing between lift coefficients of 0.4 and 0.55 was obtained with a 0.45-span leading-edge flap than with a 0.22-span leading-edge flap either without or with a fence at 0.6 span.

The addition of a 0.5-span trailing-edge flap to the wing resulted in an increase in lift coefficient at constant angle of attack (0.3 at 0° angle of attack) and an equivalent shift of the pitching-moment curve such that the wing was stable to a lift coefficient of about 0.7 (fig. 12(a)). With either one fence and the trailing-edge flap or with two fences and both the leading- and trailing-edge flaps the wing was stable to a lift coefficient of 1.0 (figs. 12(b) and 12(c)). However, the addition of the 0.5-span trailing-edge flap resulted in large unbalanced pitching moments at moderate to high lift coefficients which would require large control deflections for balance.

#### Pressure-Distribution Measurements

Pressure distributions measured at four spanwise stations on the wing are presented in figures 13, 14, and 15 for the wing, wing and fuselage, and wing and fuselage with fences at 0.6 and 0.8 semispan. Data are presented only for the lift range in which large stability changes occurred (lift coefficients from 0.4 to 0.75). The variations with angle of attack of section lift coefficient (obtained from integrated pressure distributions) for a larger lift range are shown in figure 16.

Included in figure 16 are the variations with angle of attack of pitching-moment coefficient obtained from force tests.

The pressure distributions (figs. 13 and 14) and the variations of section lift coefficient with angle of attack (fig. 16) indicate that the changes of wing stability with angle of attack shown by the pitching-moment curves in figure 16 were due principally to variations of span load distribution resulting from flow changes on the outer portion of the wing. Because of the large sweep, changes of total load on sections distant from the mean aerodynamic chord had a greater influence on the wing pitching moment than did a chordwise redistribution of load. Thus, the wing instability within the range of lift coefficients from 0.4 to 0.55 (fig. 7) can be attributed to the decrease in the rate of change of section lift coefficient with angle of attack (figs. 16(a) and 16(b)) at the outer wing sections. This decrease in lift-curve slope can be attributed to a reduction of the rate of increase of pressure coefficient on the wing with increasing angle of attack as shown in figure 17. In this figure, the pressure coefficients on the upper surface of the wing (without the fuselage, fig. 13) at several chordwise stations are presented as functions of angle of attack for the wing sections at 0.707 and 0.924 semispan.

At the angle of attack ( $3^\circ$ ) at which the slopes of the lift curves of the sections at 0.707 and 0.924 semispan decreased (figs. 16(a) and 16(b)) the pressure coefficients near the trailing edges of these sections also decreased. Observations of the flow in the boundary layer on the wing by means of tufts showed the start of spanwise flow near the trailing edge at an angle of attack of  $3^\circ$ . In reference 10, it is inferred that spanwise flow on a swept wing is a result of flow separation. Thus the decrease of pressure coefficients and the accompanying reduction of slope of the lift curve of the sections at 0.707 and 0.924 semispan are probably a result of either this separation or of the greatly increased boundary-layer thickness resulting from the flow toward the tip.

With increasing angle of attack beyond that for a lift coefficient of 0.55 ( $8^\circ$ ), the lift of the section at 0.924 semispan did not increase, while the rate of change of lift with angle of attack of the section at 0.707 semispan increased (figs. 16(a) and 16(b)). The increase in the slope of the lift curve of the section at 0.707 semispan between angles of attack of  $8^\circ$  and about  $11^\circ$  can be attributed to the increase in pressure coefficients over the after portion of the section within this angle-of-attack range as may be seen in figure 13. From the shape of the chordwise pressure distributions of the section at 0.707 semispan above an angle of attack of  $11^\circ$  (figs. 13 and 14), it is surmised that a region of separated flow existed near the wing leading edge with reattachment of the flow farther downstream on the wing. In reference 11, studies of tufts on an airfoil which had a similar type of flow separation and reattachment indicated that within the separated region a circulatory motion existed strongly suggestive of a vortex. On the wing of the present

investigation, the increase in section lift-curve slope of the section at 0.707 semispan may have been induced by this vortex in the separated flow region. These increases in the rate of change of lift coefficient with angle of attack resulted in a stable pitching-moment variation between lift coefficients of 0.55 and 0.75.

Further increases in angle of attack finally resulted in an abrupt loss in lift at station 0.707, giving the unstable pitching-moment variation above a lift coefficient of 0.75.

The effect of fences at 0.6 and 0.8 semispan on the wing pressure distribution is shown in figure 15. The fences altered the spanwise boundary-layer flow sufficiently so that lift on the tip (station 0.924) was maintained to higher angles of attack as shown in figure 16. This resulted in a considerable improvement in the longitudinal stability between lift coefficients of 0.4 and 0.6 (fig. 10(a)).

#### Comparison of Theoretical and Experimental Span Loading

Methods of computing the span load distribution of twisted and cambered swept wings have been developed in references 3, 12, and 13. As a check on the accuracy of these methods the span loading of the twisted and cambered  $63^\circ$  swept-back wing (without a fuselage) was computed and compared with the measured loading. The comparison is shown in figure 18 for the basic loading (due to the camber and twist) and for the basic plus additional loading (due to angle of attack) for a lift coefficient of 0.4. The latter comparison is made for a lift coefficient at which local flow separation had not affected the span loading appreciably. It is indicated in figure 18 that good agreement was obtained between the computed and the experimental span load distributions for these conditions.

#### CONCLUDING REMARKS

The results of tests at low speed showed that the longitudinal-stability characteristics of a wing with the leading edge swept back  $63^\circ$  were not improved through the use of this particular twist and camber. Large variations in stability with lift coefficient of the wing were attributed to flow separation and to thickening of the boundary layer near the tip. The twisted and cambered wing had the higher lift-drag ratio above a lift coefficient of 0.3.

The addition of flaps and fences to the wing delayed the effects of spanwise flow and the thickening of the boundary layer on the twisted and cambered wing to higher lift coefficients. The wing with upper-surface fences and a leading-edge flap was longitudinally stable to a lift

coefficient of about 0.8. Addition of a trailing-edge flap extended the range over which the wing was longitudinally stable to a lift coefficient of 1.0 with, however, a considerable increase of the unbalanced pitching moments.

Within the angle-of-attack range in which flow separation did not affect appreciably the lift at any section, good agreement was obtained between the measured span load distribution and that computed by the methods of Weissinger.

Ames Aeronautical Laboratory,  
National Advisory Committee for Aeronautics,  
Moffett Field, Calif.

#### REFERENCES

1. McCormack, Gerald M., and Walling, Walter C.: Aerodynamic Study of a Wing-Fuselage Combination Employing a Wing Swept Back  $63^{\circ}$ . - Investigation of a Large-Scale Model at Low Speed. NACA RM A8D02, 1949.
2. Hopkins, Edward J.: Aerodynamic Study of a Wing-Fuselage Combination Employing a Wing Swept Back  $63^{\circ}$ . - Effects of Split Flaps, Elevons, and Leading-Edge Devices at Low Speed. NACA RM A9C21, 1949.
3. Stevens, Victor I.: Theoretical Basic Span Loading Characteristics of Wings with Arbitrary Sweep, Aspect Ratio, and Taper Ratio. NACA TN 1772, 1948.
4. Swanson, Robert S., and Toll, Thomas A.: Jet-Boundary Corrections for Reflection-Plane Models in Rectangular Wind Tunnels. NACA Rep. 770, 1943.
5. Polhamus, Edward C.: Jet-Boundary-Induced-Upwash Velocities for Swept Reflection-Plane Models Mounted Vertically in 7- by 10-foot Closed, Rectangular Wind Tunnels. NACA TN 1752, 1948.
6. Reynolds, Robert M., and Smith, Donald W.: Aerodynamic Study of a Wing-Fuselage Combination Employing a Wing Swept Back  $63^{\circ}$ . - Subsonic Mach and Reynolds Number Effects on the Characteristics of the Wing and on the Effectiveness of an Elevon. NACA RM A8D20, 1949.
7. Jones, Robert T.: Estimated Lift-Drag Ratios at Supersonic Speed. NACA TN 1350, 1947.

8. Graham, Robert R., and Conner, D. William: Investigation of High-Lift and Stall-Control Devices on an NACA 64-Series 42° Sweptback Wing With and Without Fuselage. NACA RM L7G09, 1947.
9. Conner, D. William, and Neely, Robert H.: Effects of a Fuselage and Various High-Lift and Stall-Control Flaps on Aerodynamic Characteristics in Pitch of an NACA 64-Series 40° Swept-Back Wing. NACA RM L6L27, 1947.
10. Jones, Robert T.: Effects of Sweepback on Boundary Layer and Separation. NACA Rep. 884, 1947.
11. Gault, Donald E.: Boundary-Layer and Stalling Characteristics of the NACA 63-009 Airfoil Section. NACA TN 1894, 1949.
12. Weissinger, J.: The Lift Distribution of Swept-Back Wings. NACA TM 1120, 1947.
13. DeYoung, John: Theoretical Additional Span Loading Characteristics of Wings with Arbitrary Sweep, Aspect Ratio, and Taper Ratio. NACA TN 1491, 1947.

TABLE I.— DIMENSIONS OF THE SEMISPAN MODEL

Wing	
Area, square feet . . . . .	14.262 <sup>a</sup>
Span, feet . . . . .	5.0
Mean aerodynamic chord, feet . . . . .	3.20
Aspect ratio . . . . .	3.5 <sup>b</sup>
Taper ratio . . . . .	0.25
Sweepback of leading edge, degrees . . . . .	63
Sweepback of 1/4-chord line, degrees . . . . .	60.8
Geometric twist, degrees . . . . .	18
Dihedral, degrees . . . . .	0
Fuselage	
Length, feet . . . . .	14.2
Maximum diameter, feet . . . . .	1.36
Fineness ratio . . . . .	10.4

<sup>a</sup>Area to projected tip was 14.286 square feet.

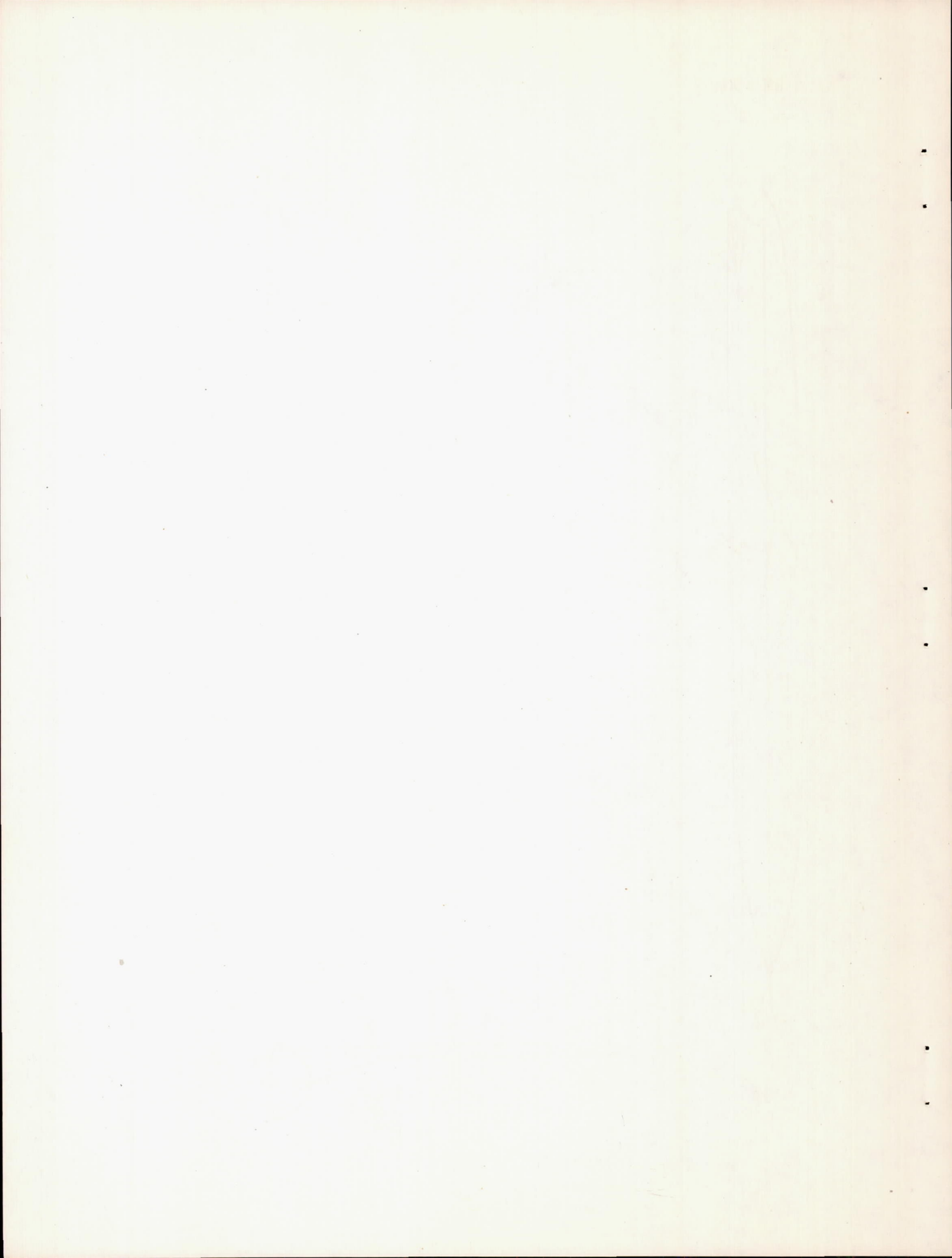
<sup>b</sup>Based on dimensions of complete wing and area to projected tip.



TABLE II.— COORDINATES OF THE FUSELAGE  
 [ All dimensions in inches ]

Station	Diameter	Station	Diameter
0	0	81.6	16.32
4	2.84	91.8	16.20
8	5.34	102.0	15.82
12	7.50	112.2	15.20
16	9.30	122.4	14.28
20	10.80	132.6	13.26
24	11.98	142.8	11.68
28	12.88	153.0	9.86
30.6	13.26	163.2	7.58
40.8	14.28	164.4	7.16
51.0	15.20	166.4	5.82
61.2	15.82	168.4	3.58
71.4	16.20	170.4	0
Fineness ratio, $\frac{\text{length}}{\text{maximum diameter}} = 10.4$			





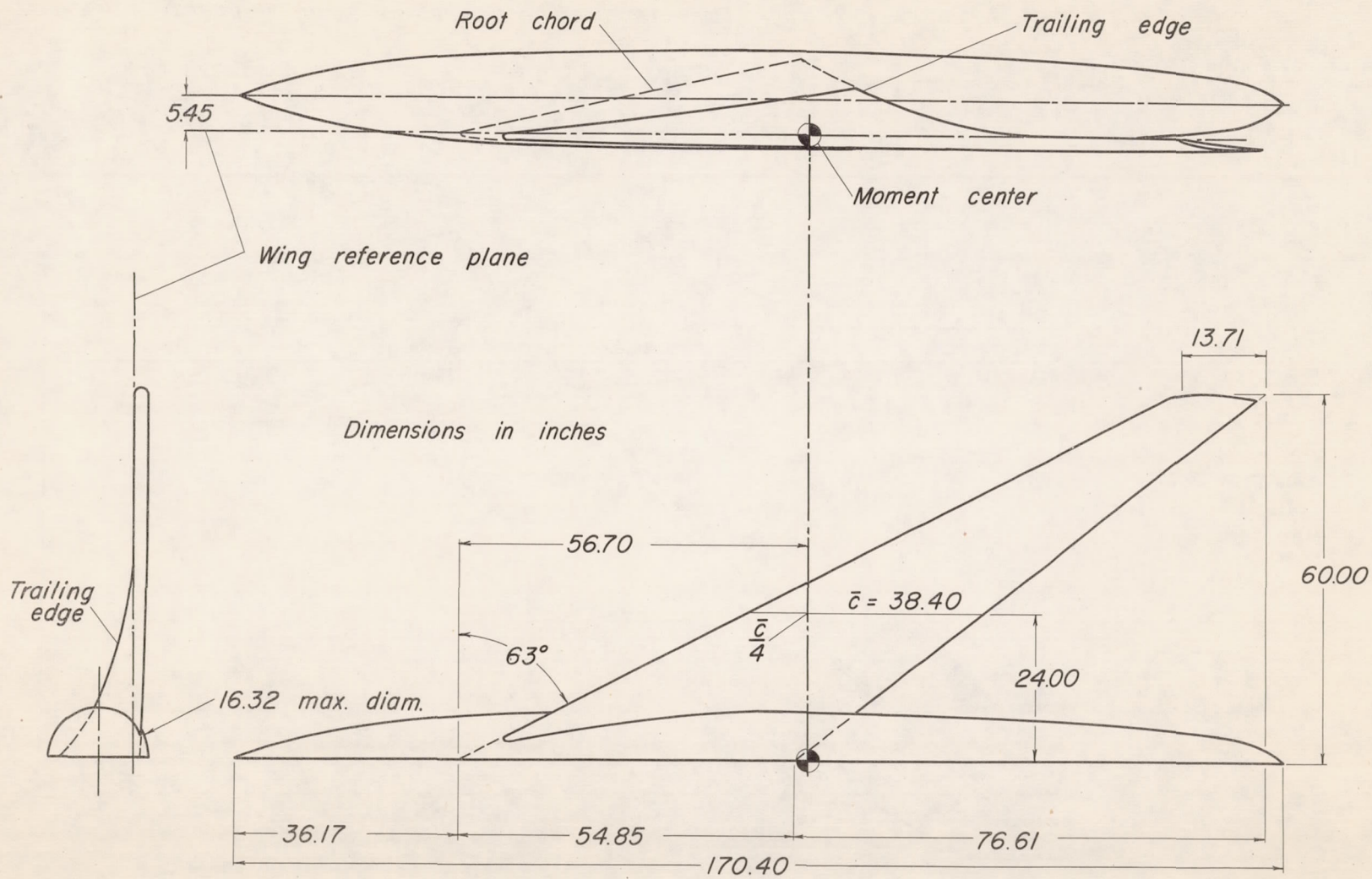


Figure 1.— Diagram of the model.

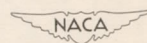


FIGURE 2.—Relationship between the wing geometry and the coordinate axes.

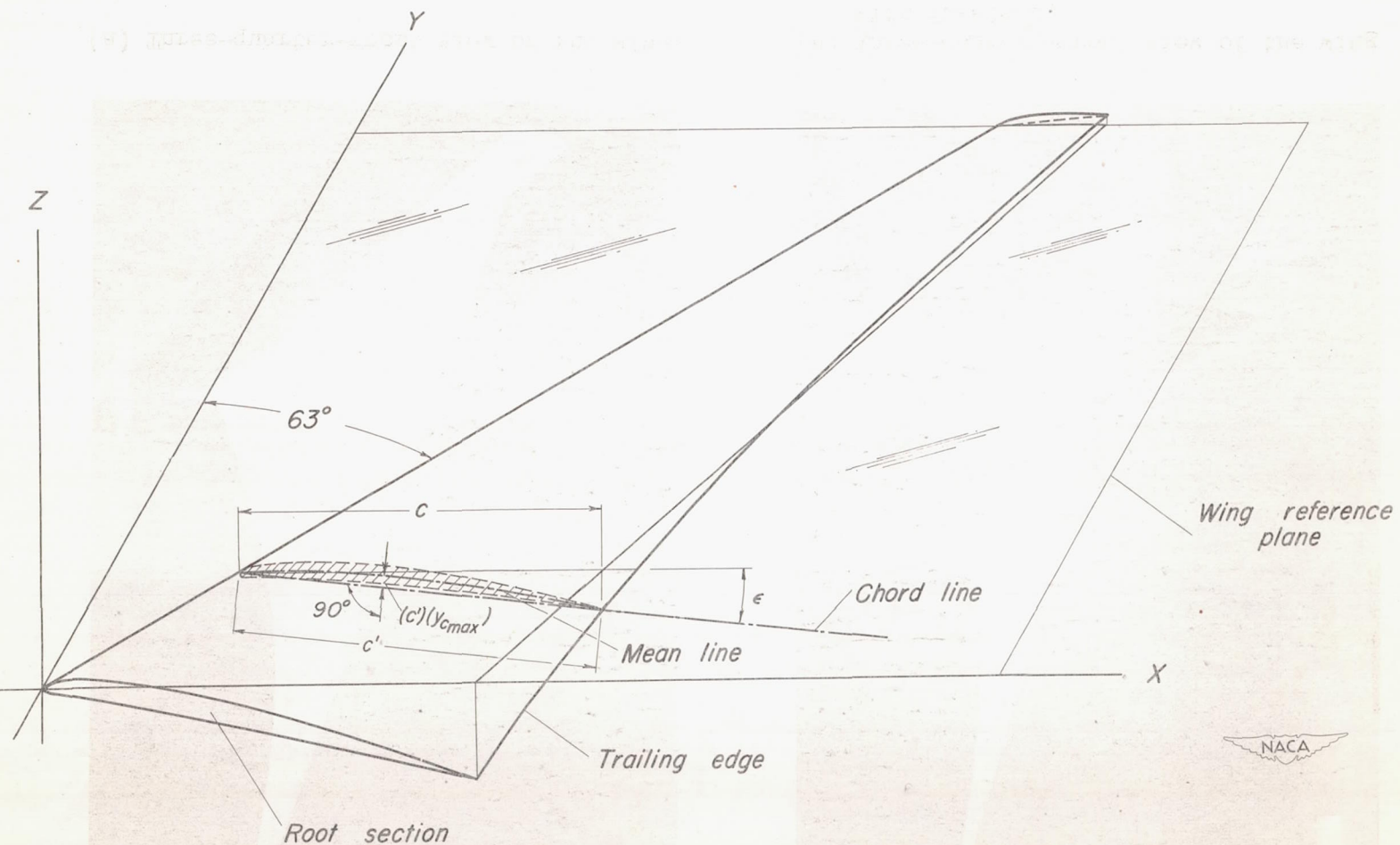
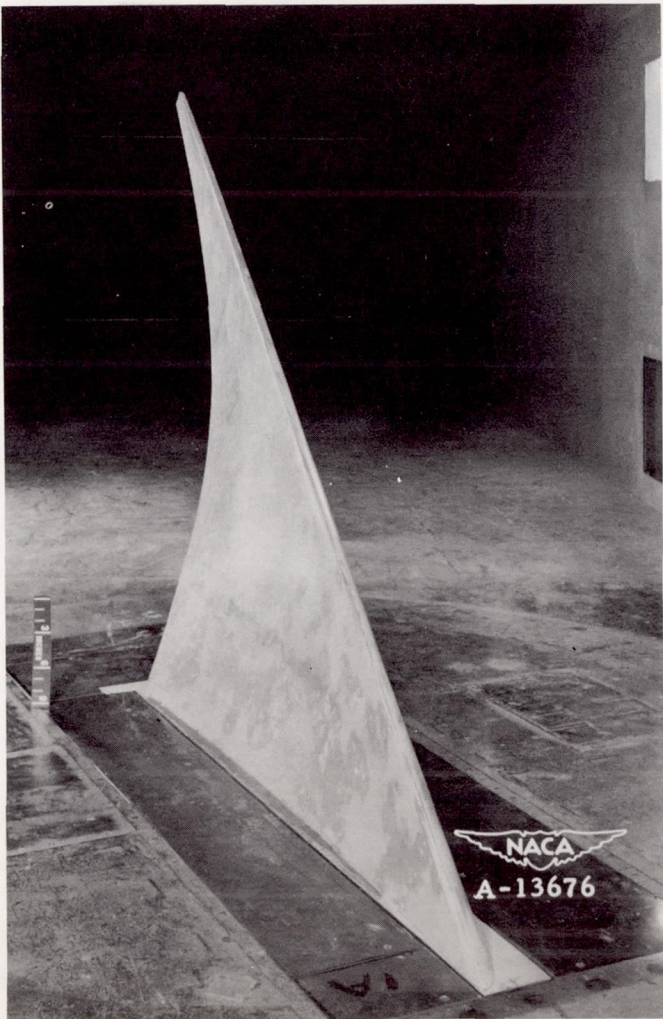
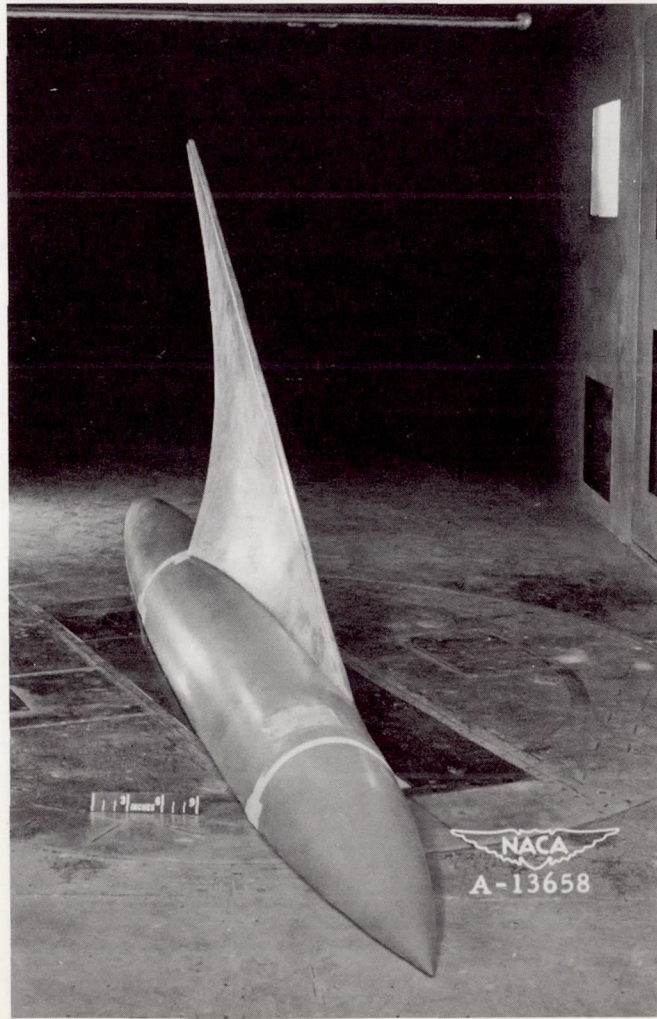


Figure 2.—Relationship between the wing geometry and the coordinate axes.

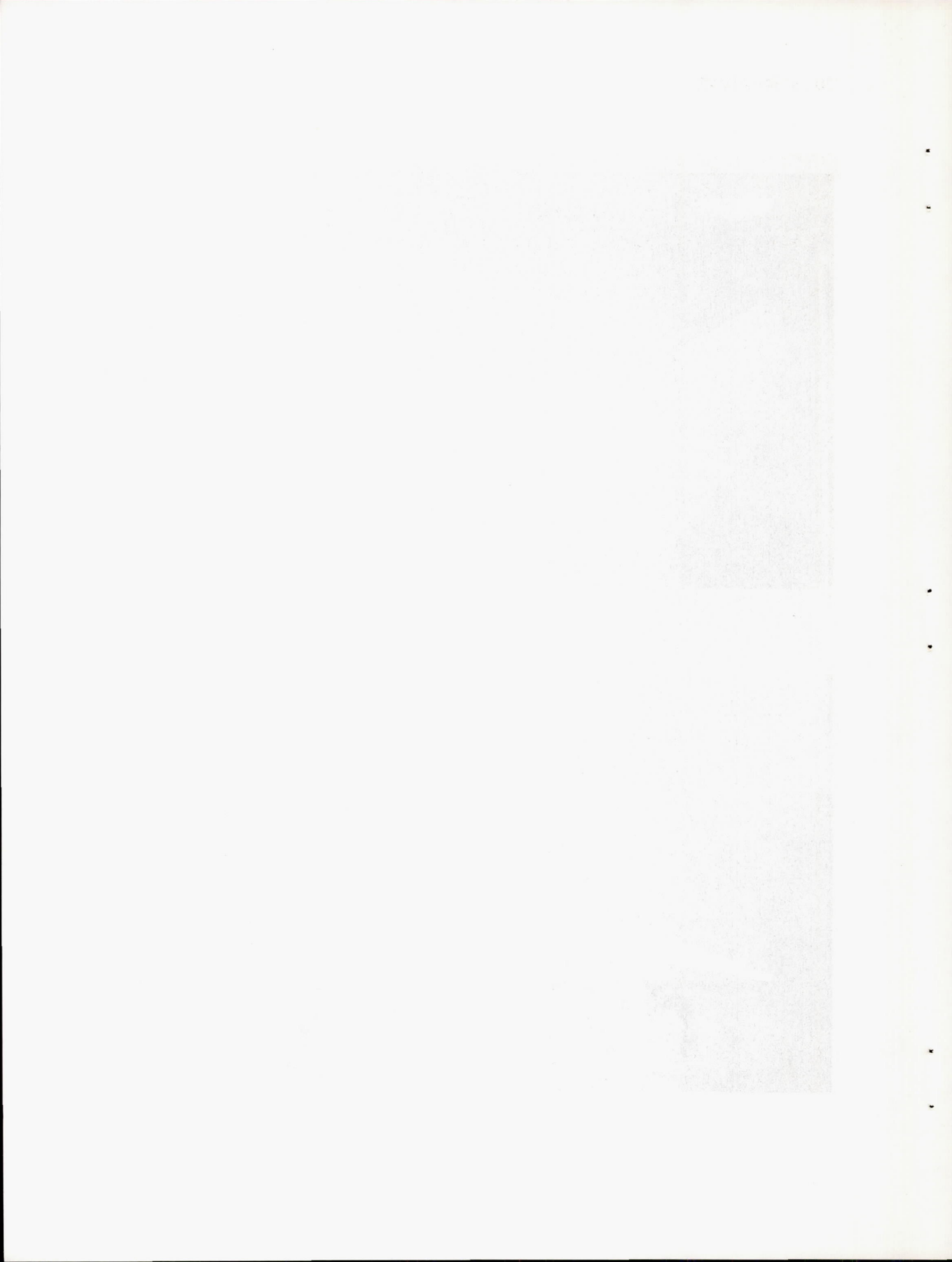


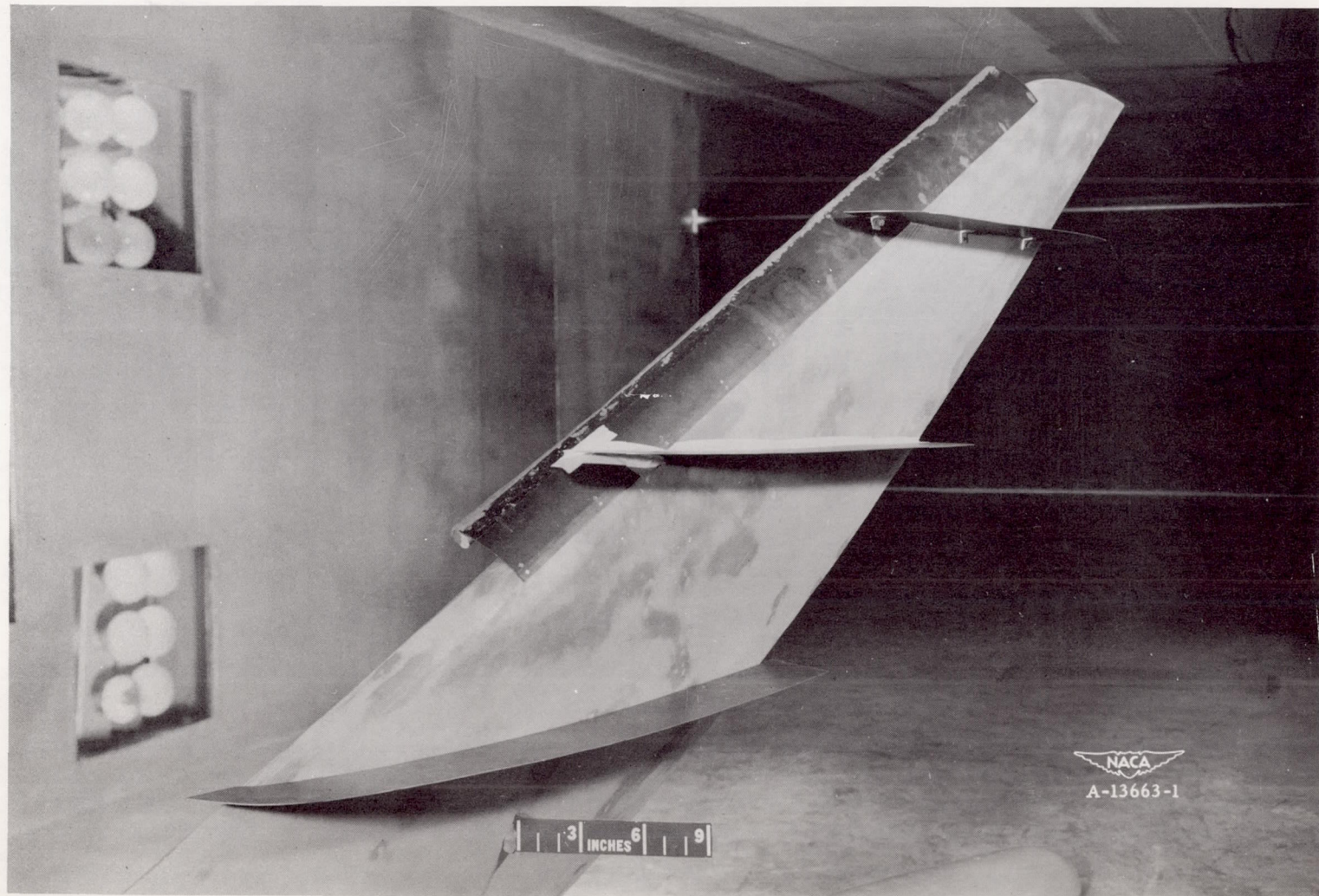
(a) Three-quarter-front view of the wing.



(b) Three-quarter-front view of the wing with fuselage.

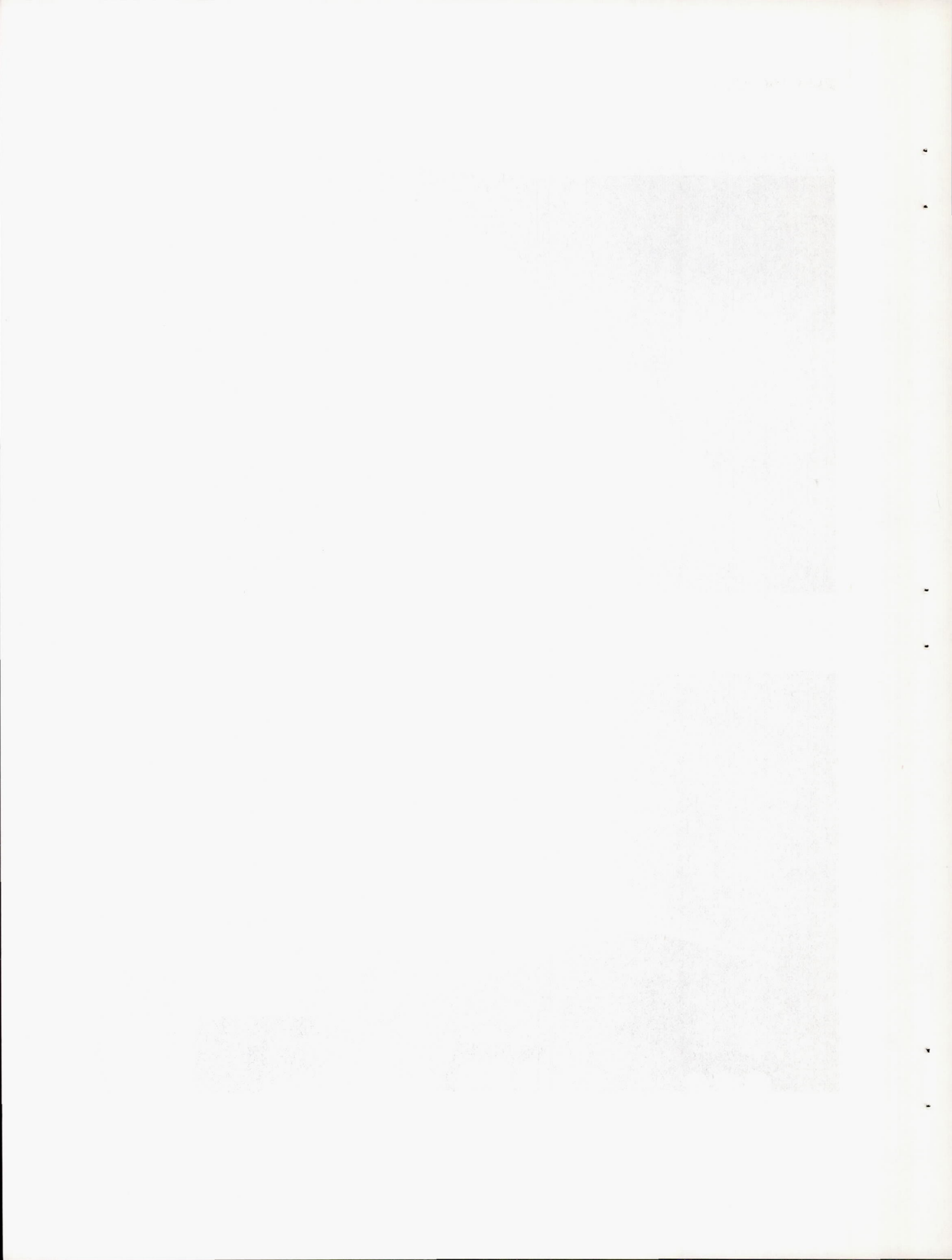
Figure 3.- The model mounted in the wind tunnel.

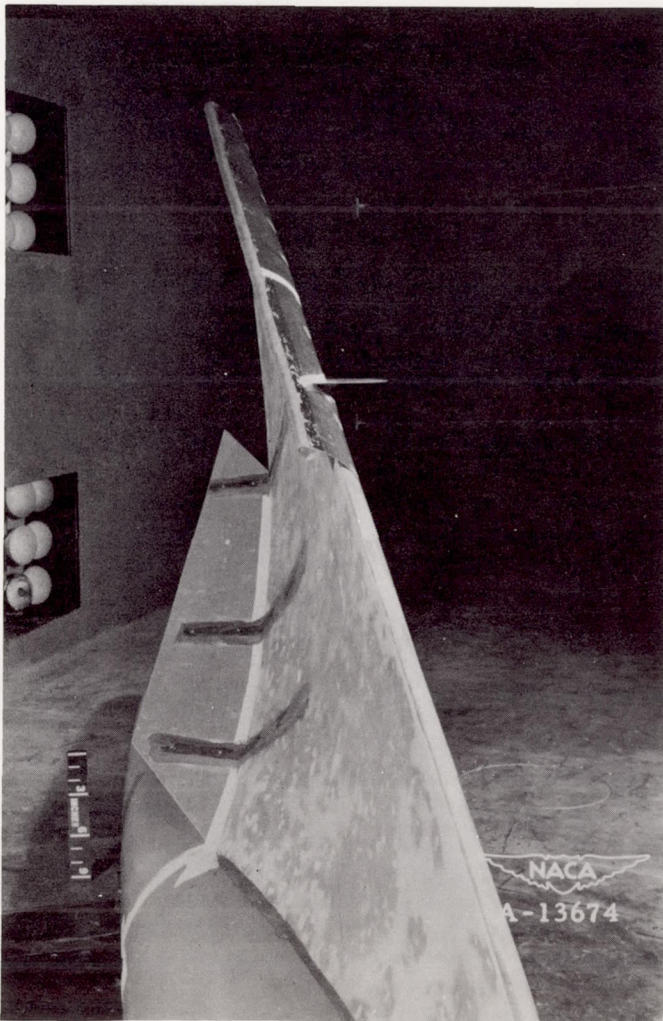




(c) Wing with fences and 0.45-span leading-edge flap.

Figure 3.- Continued.



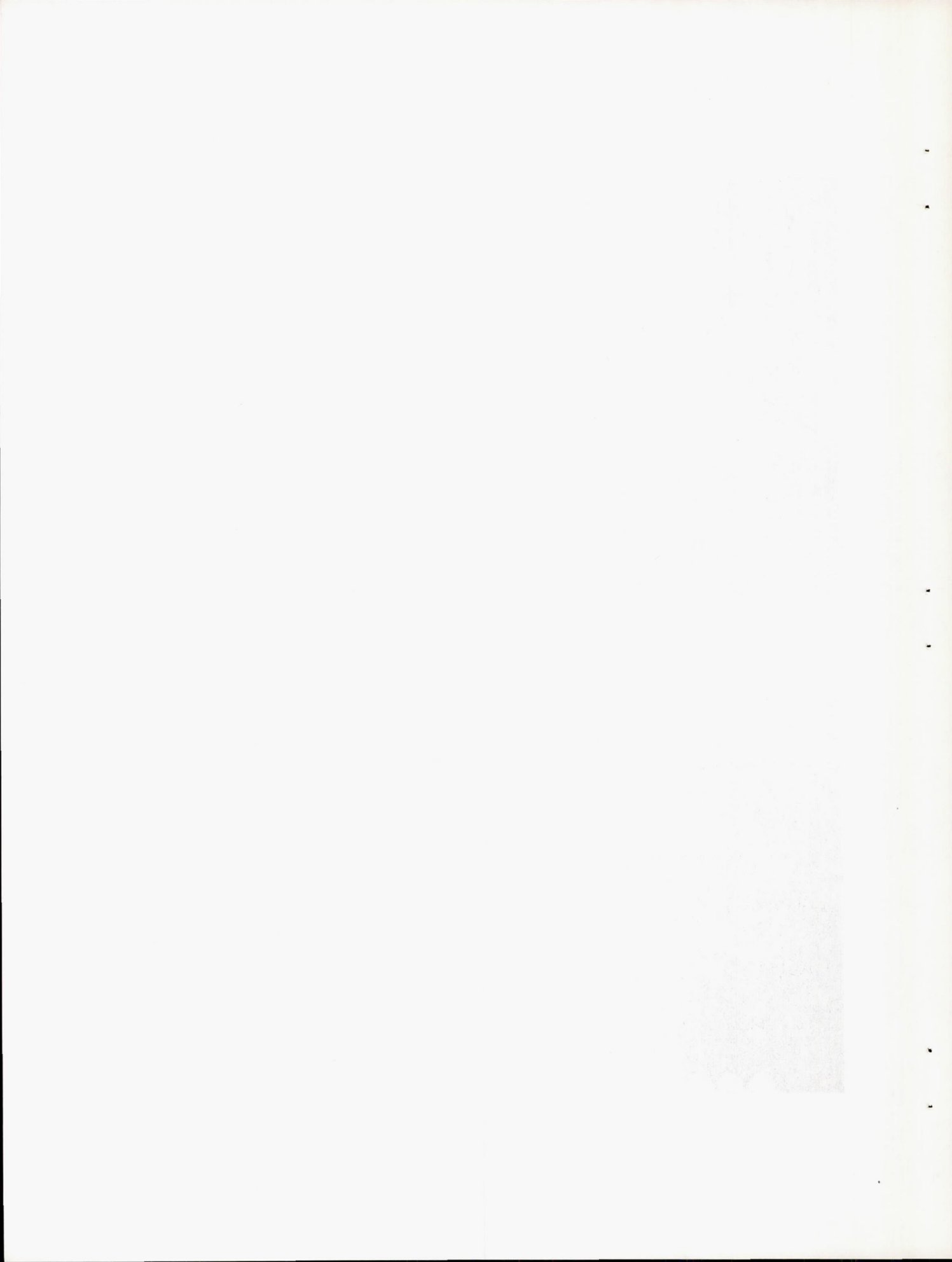


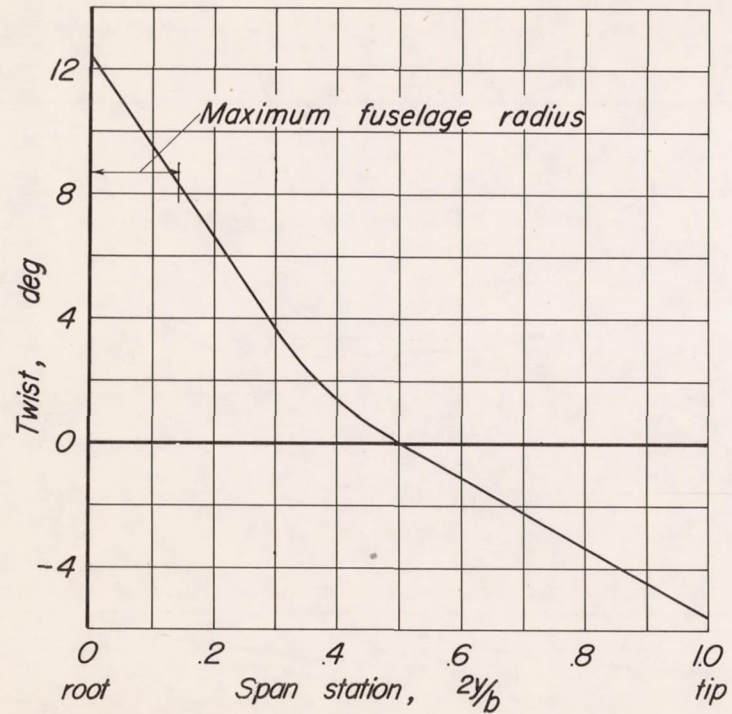
(d) Front view of the wing showing the leading- and trailing-edge flaps.

Figure 3.- Concluded.

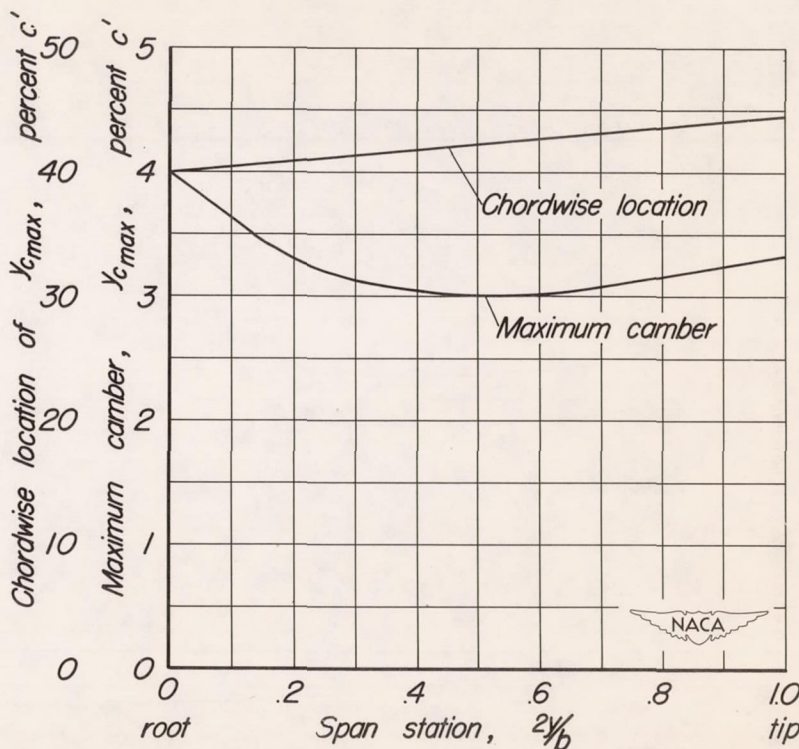


(e) Three-quarter-front view of the wing showing the leading- and trailing-edge flaps.



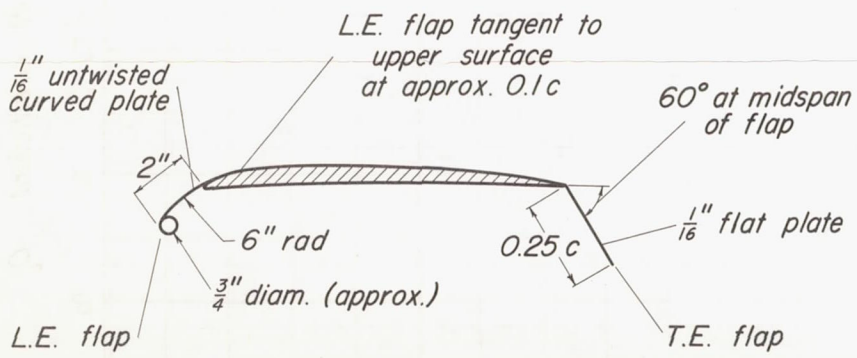
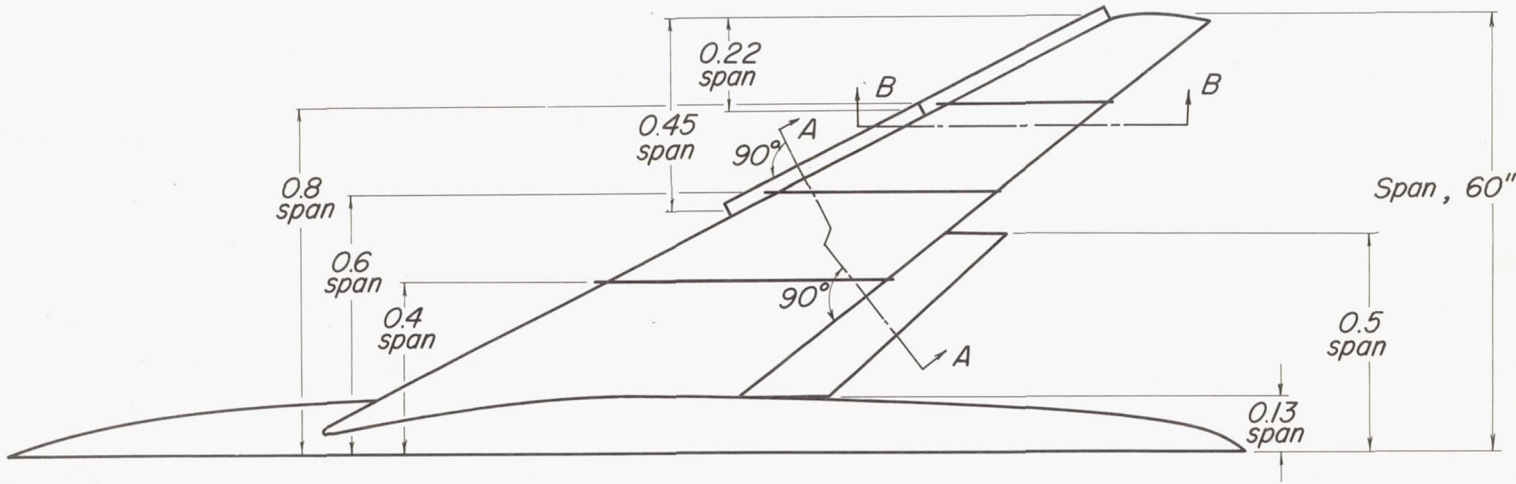


(a) Twist.

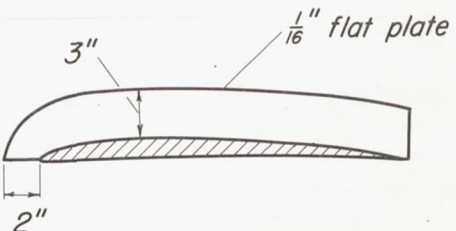


(b) Maximum camber and chordwise location.

Figure 4.-Spanwise variation of twist and camber of the model.



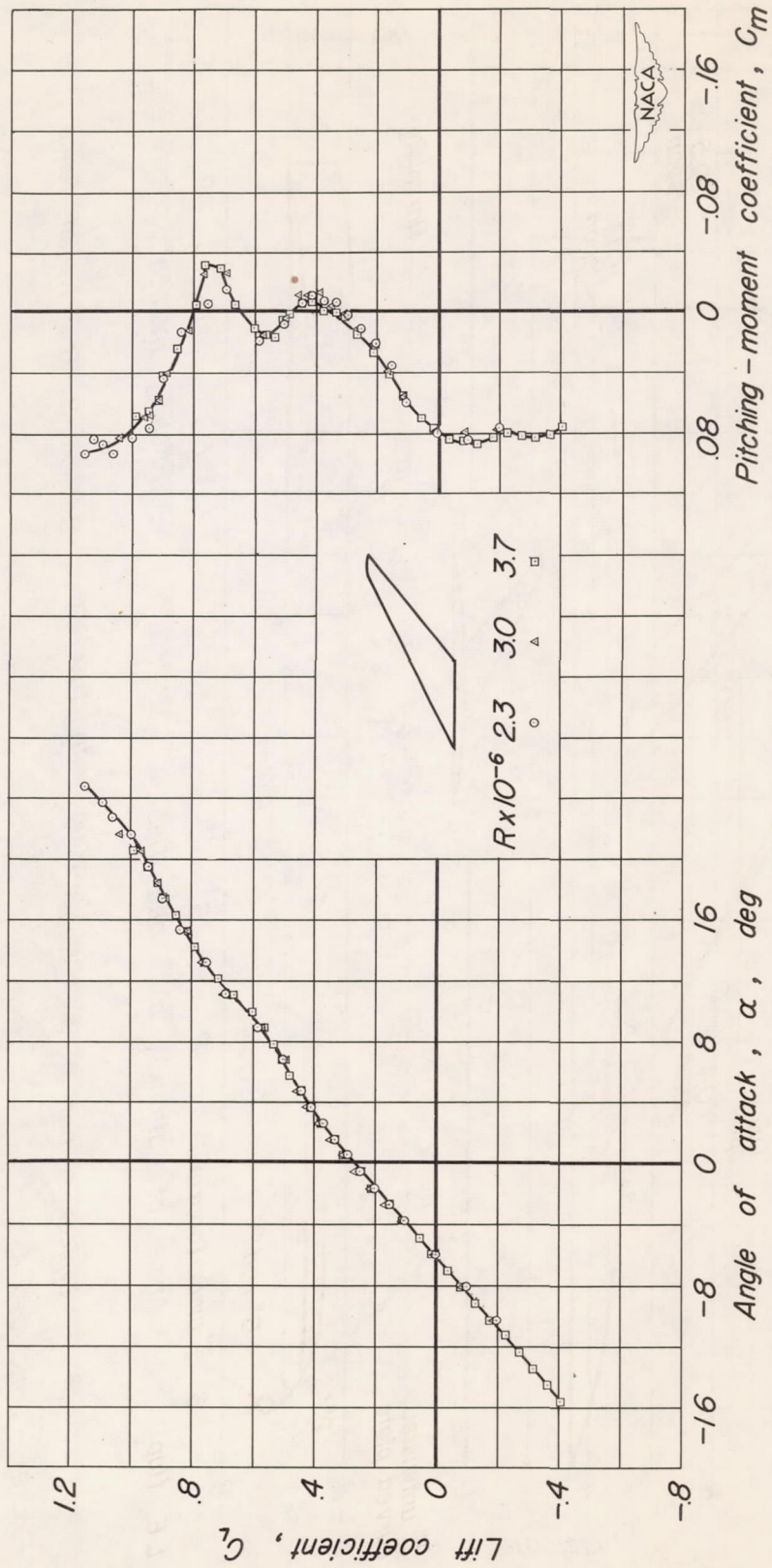
Typical section A-A, flaps



Section B-B, typical fence



Figure 5.— Geometry of the flaps and the fences.



(a) Wing.

Figure 6:- Effect of Reynolds number.

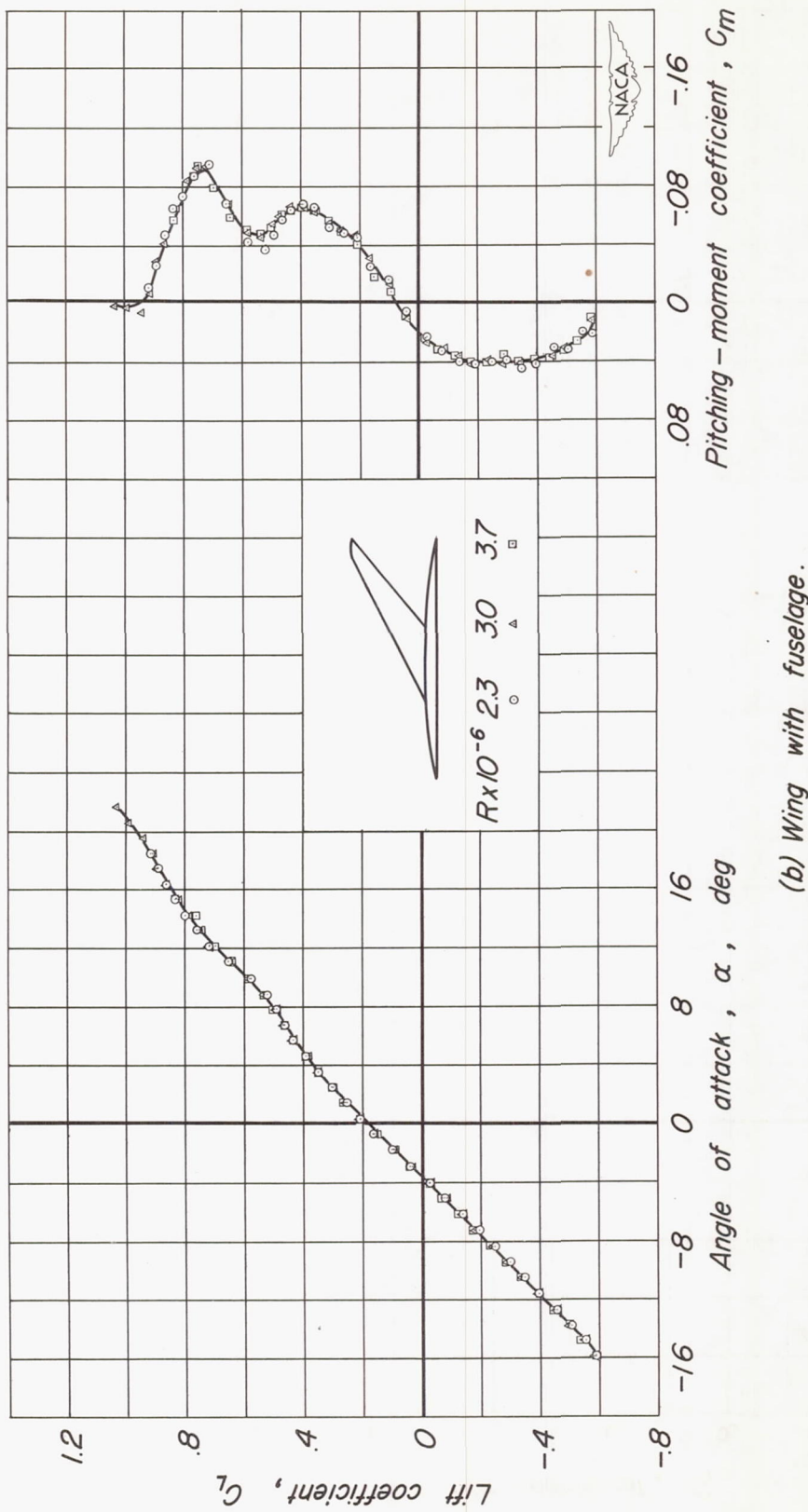


Figure 6:- Concluded.

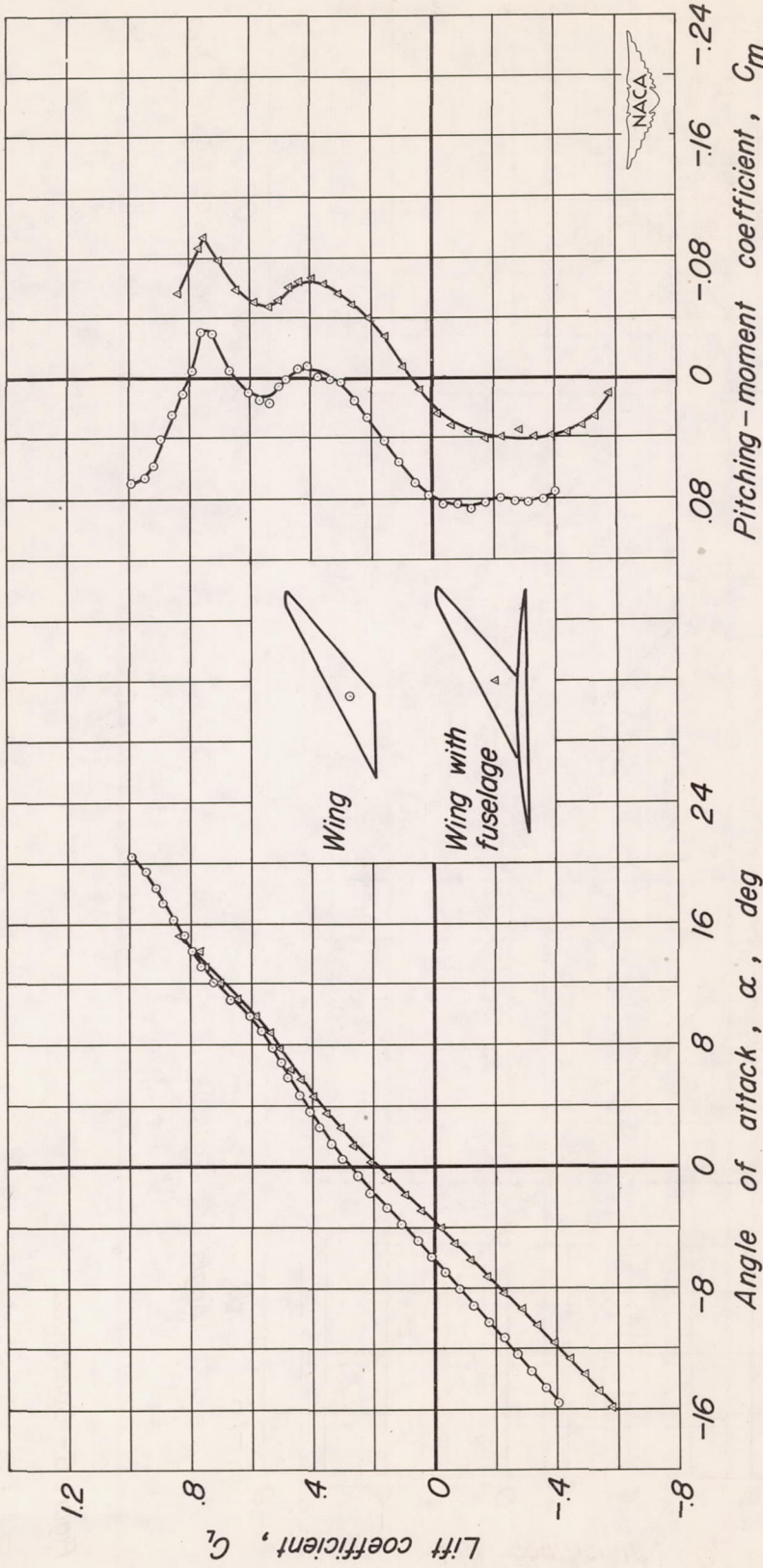
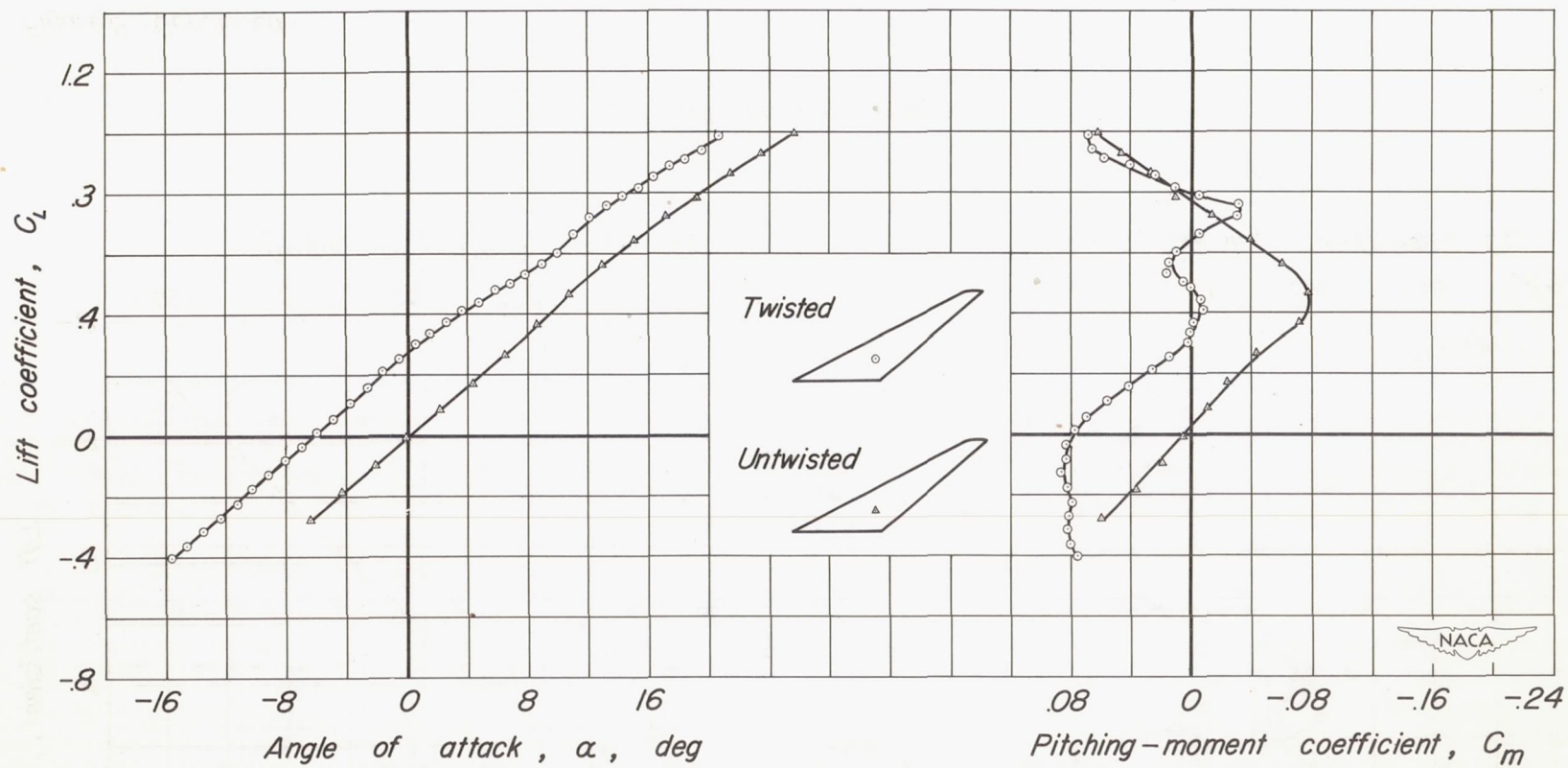
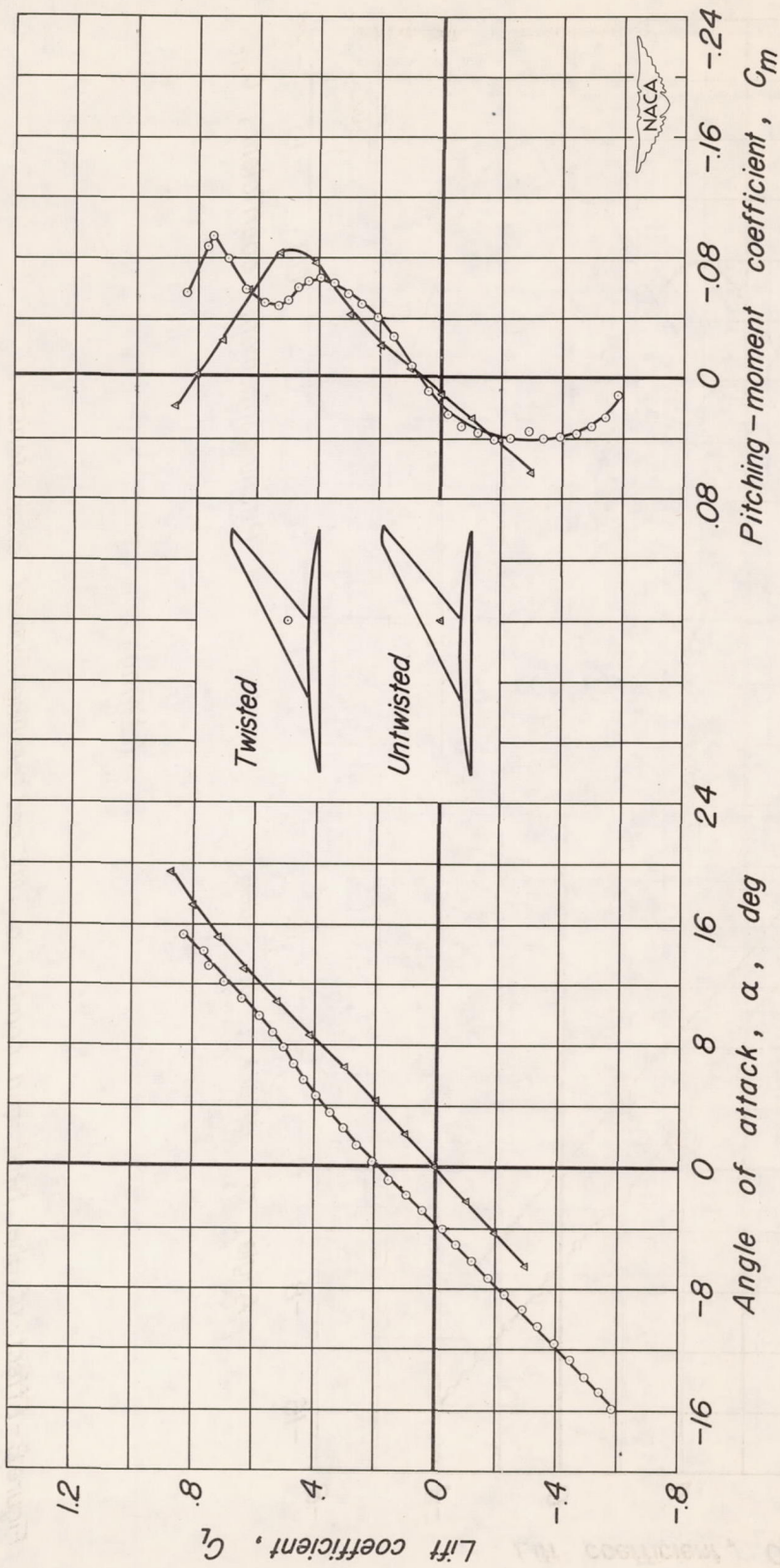


Figure 7-Effect of a fuselage.



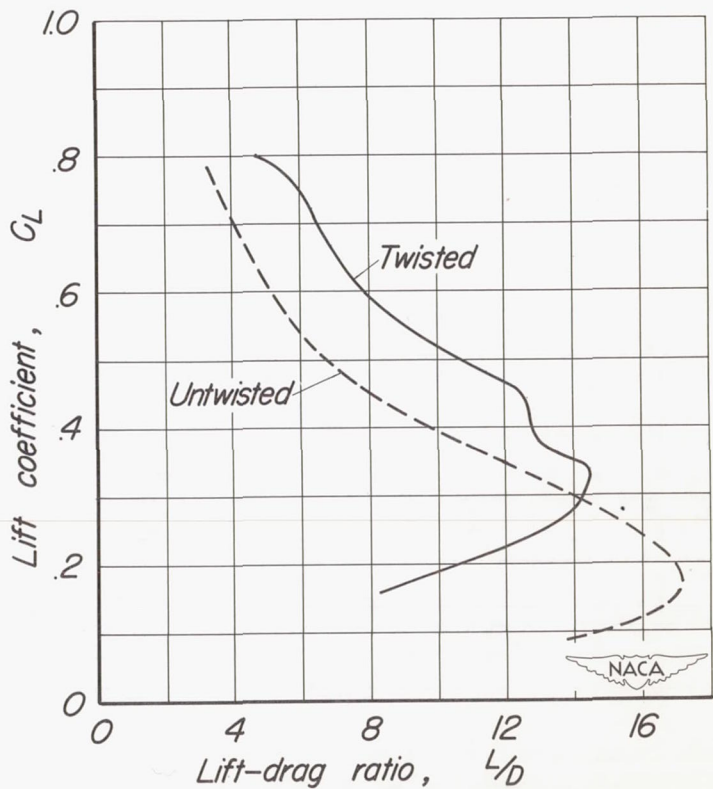
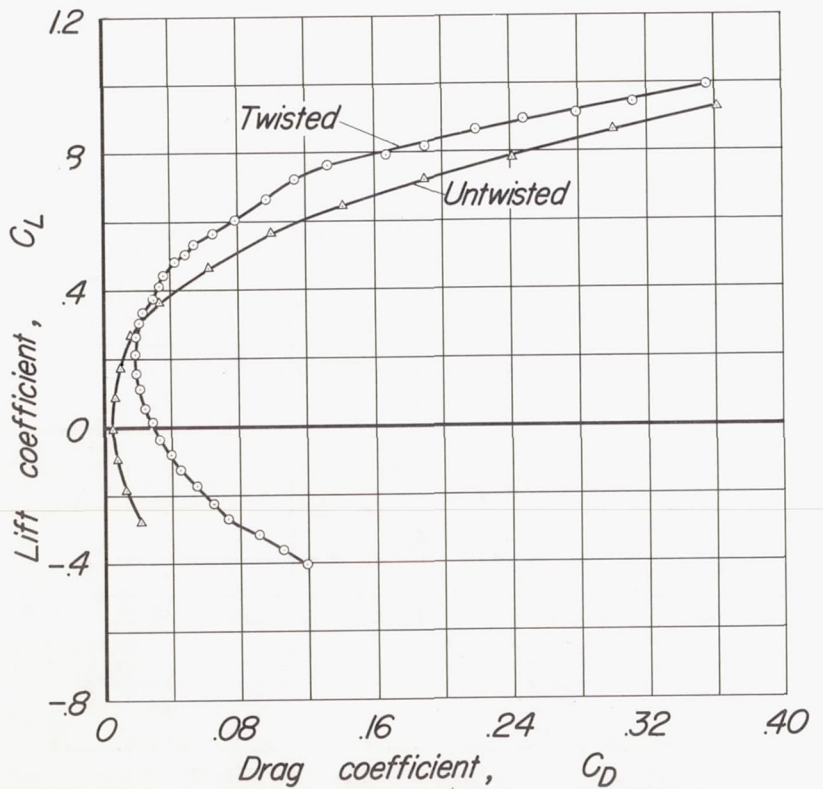
(a) Wing.

Figure 8.-Effect of the twist and camber on lift and pitching-moment characteristics.



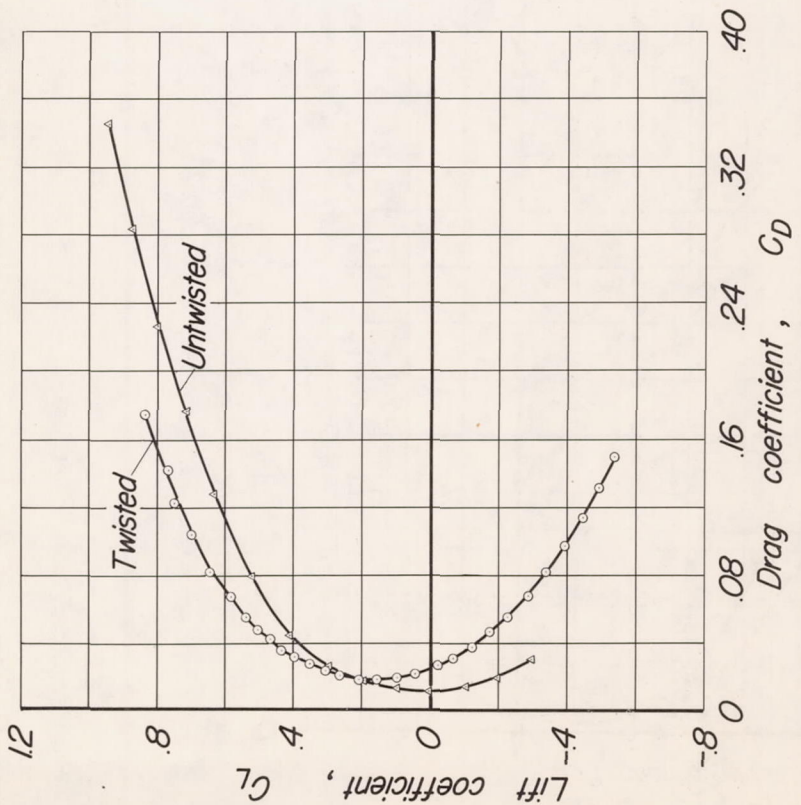
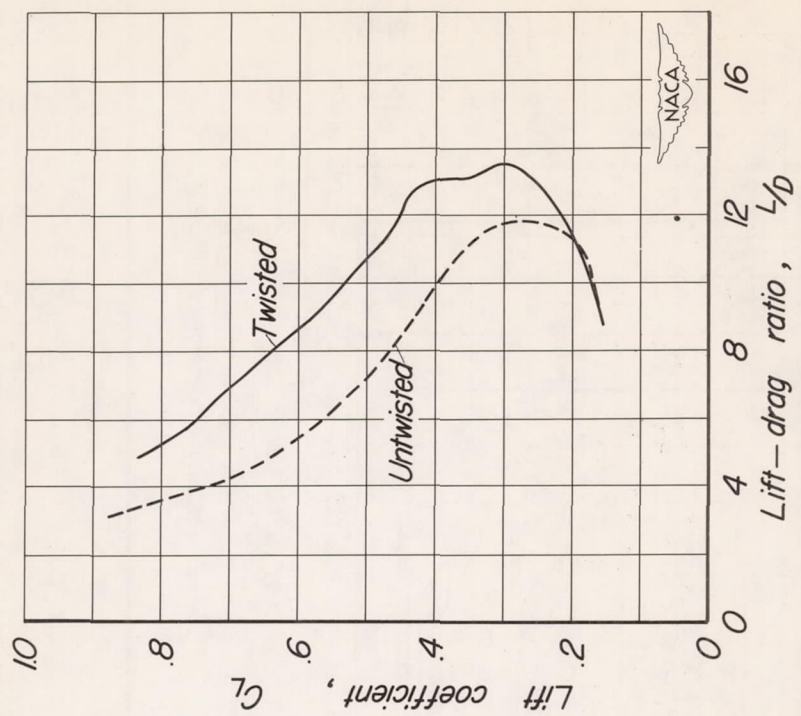
(b) Wing with fuselage.

Figure 8.-Concluded.



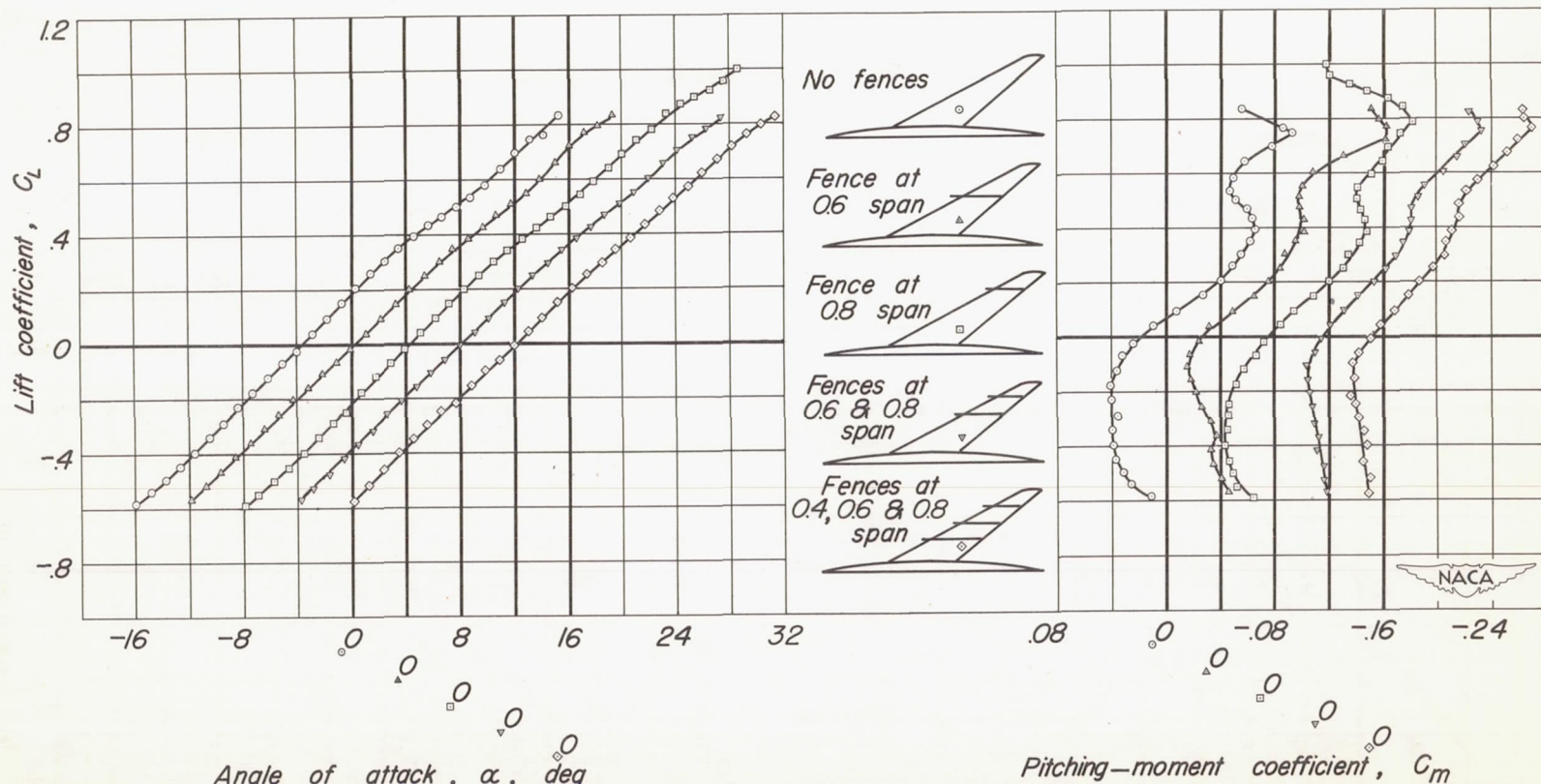
(a)Wing.

Figure 9.-Effect of the twist and camber on drag characteristics.



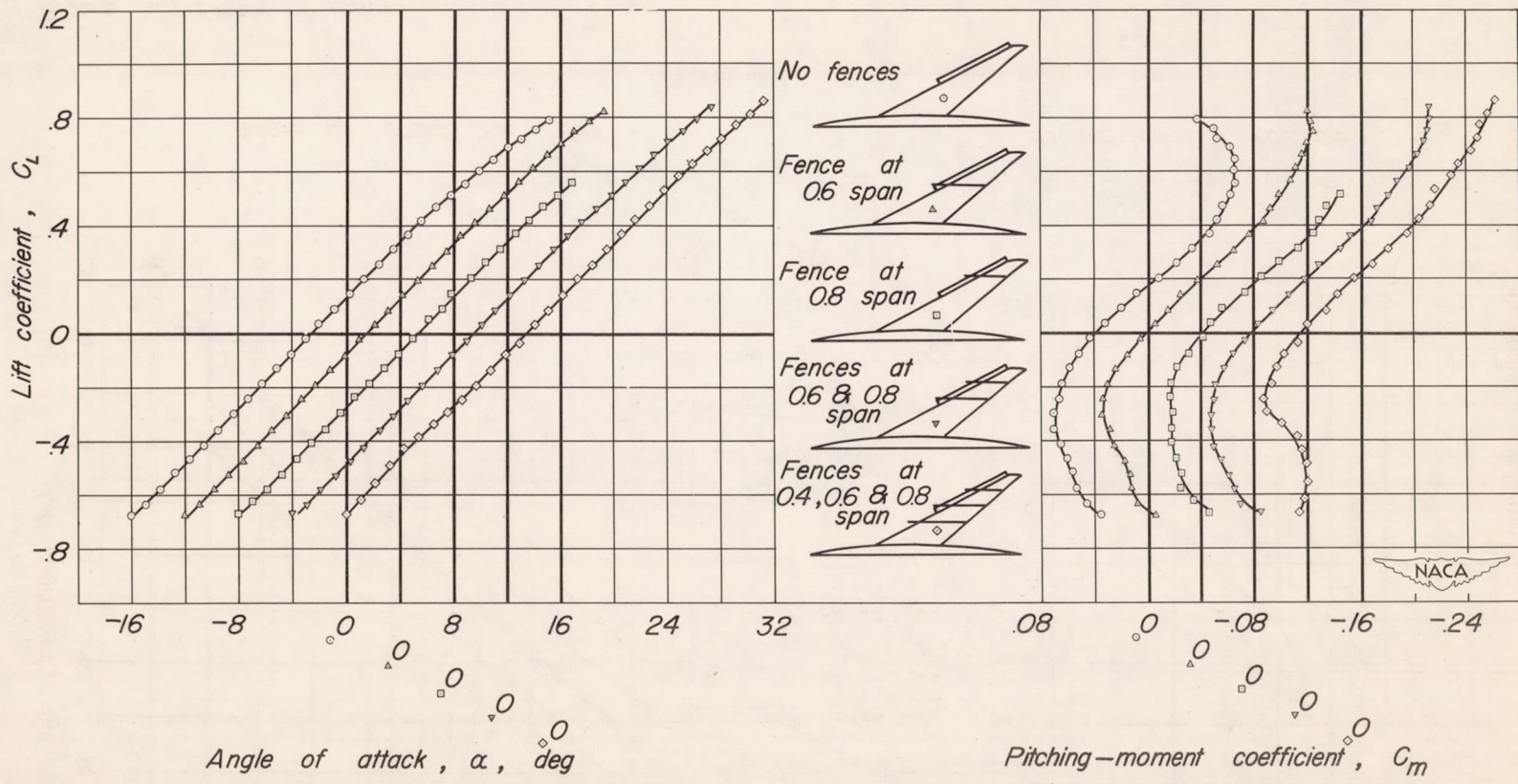
(b) Wing with fuselage.

Figure 9-Concluded.



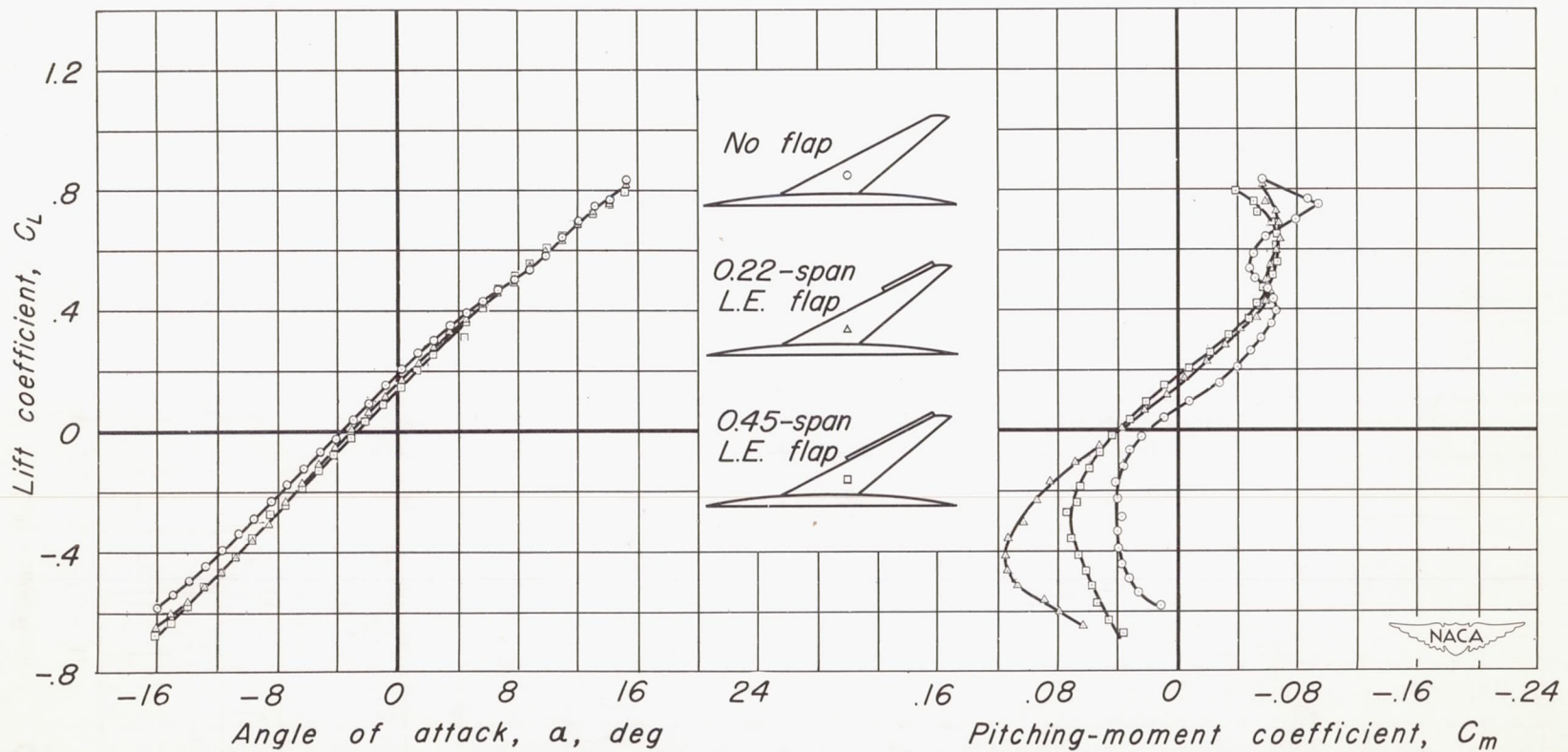
(a) Without a leading-edge flap.

Figure 10.- Effect of fences.



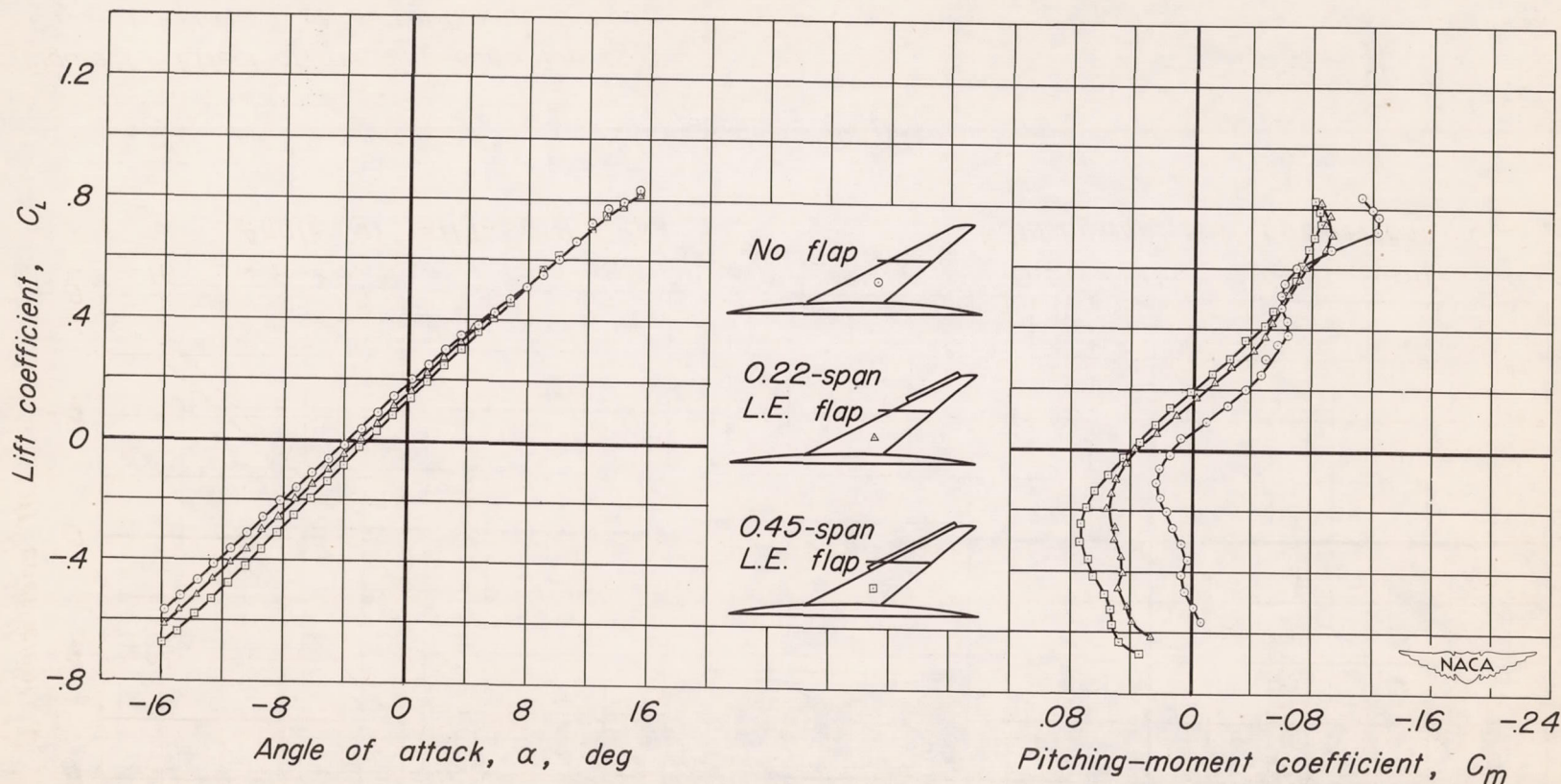
(b) With a 0.45-span leading-edge flap.

Figure 10.—Concluded.



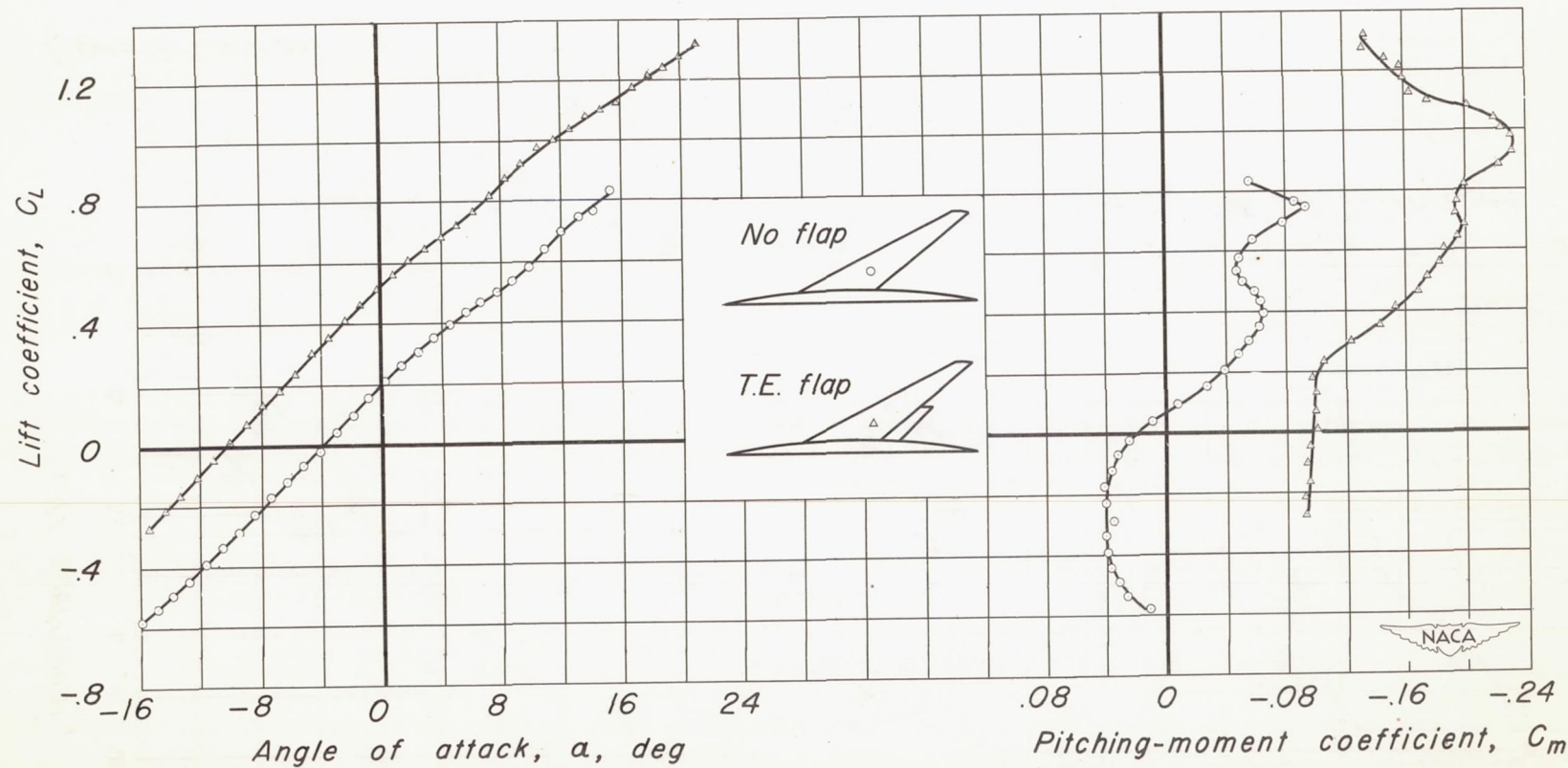
(a) Without fences.

Figure 11.—Effect of leading-edge flap span.



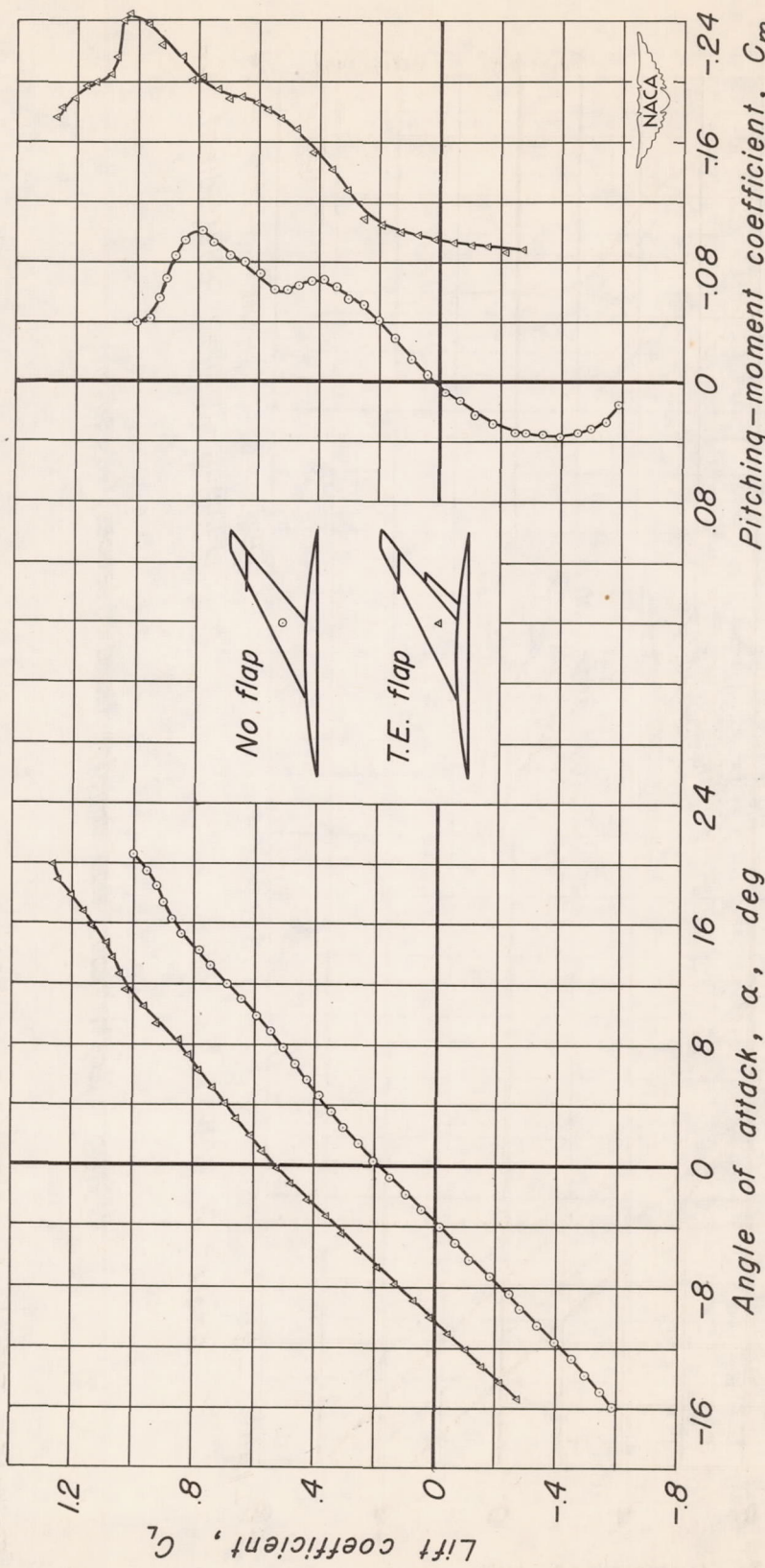
(b) With a fence at 0.6 span.

Figure 11- Concluded.



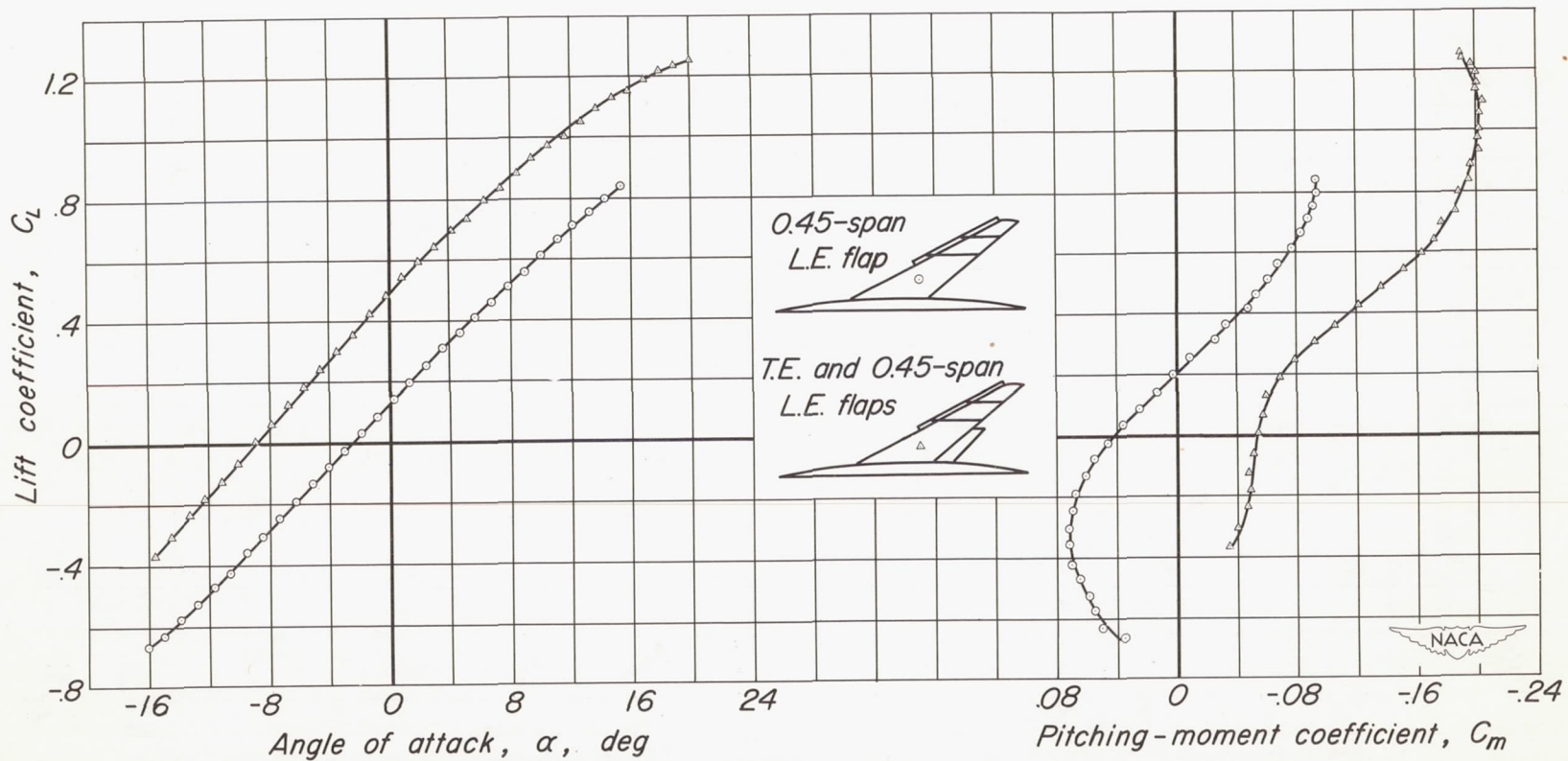
(a) Without leading-edge flaps or fences.

Figure 12.- Effect of a trailing-edge flap.



(b) With a fence at 0.8 span.

Figure 12.—Continued.



(a) With a leading-edge flap and fences at 0.6 and 0.8 span.

Figure 12.— Concluded.

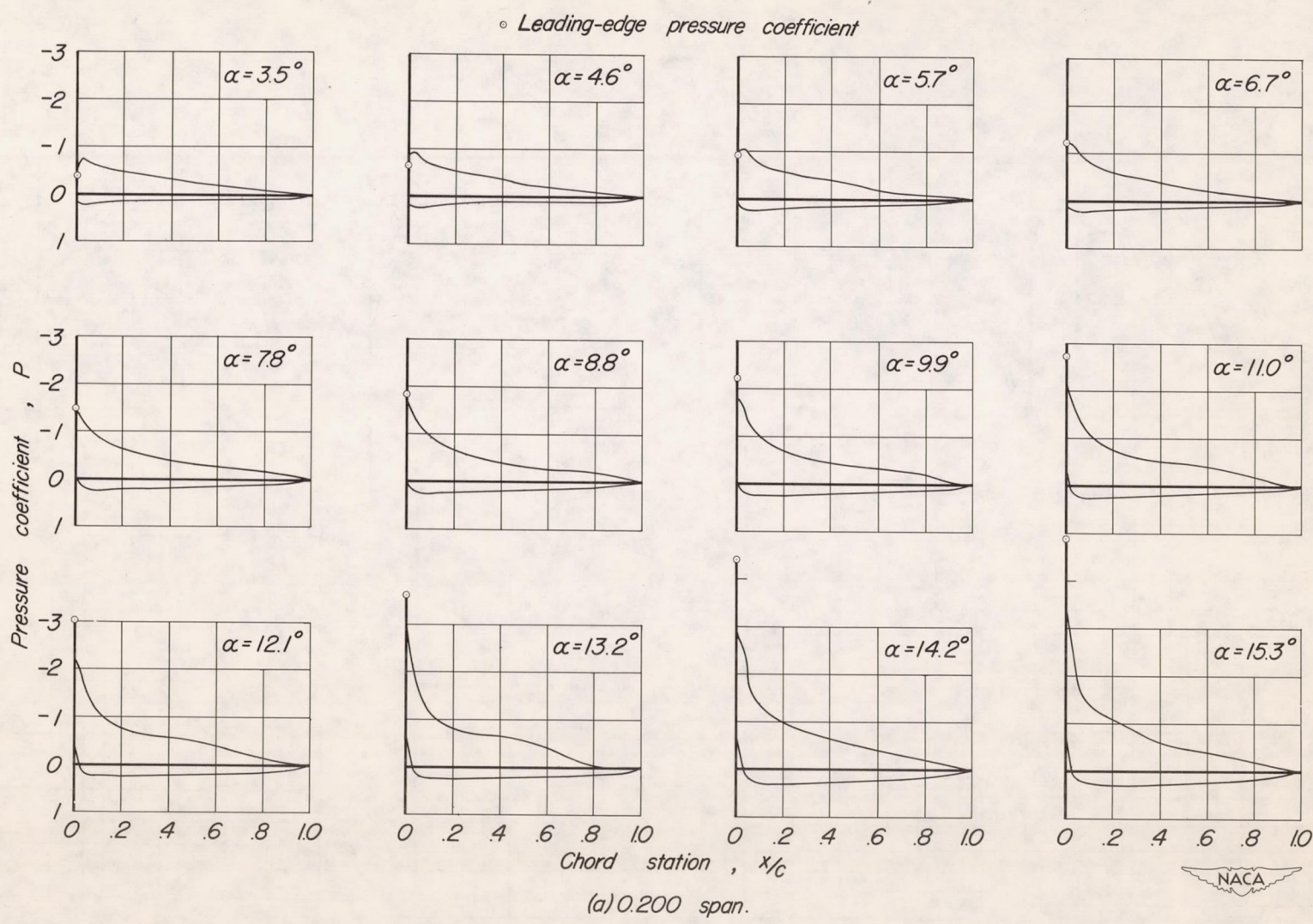


Figure 13.-Chordwise pressure distribution on the wing.

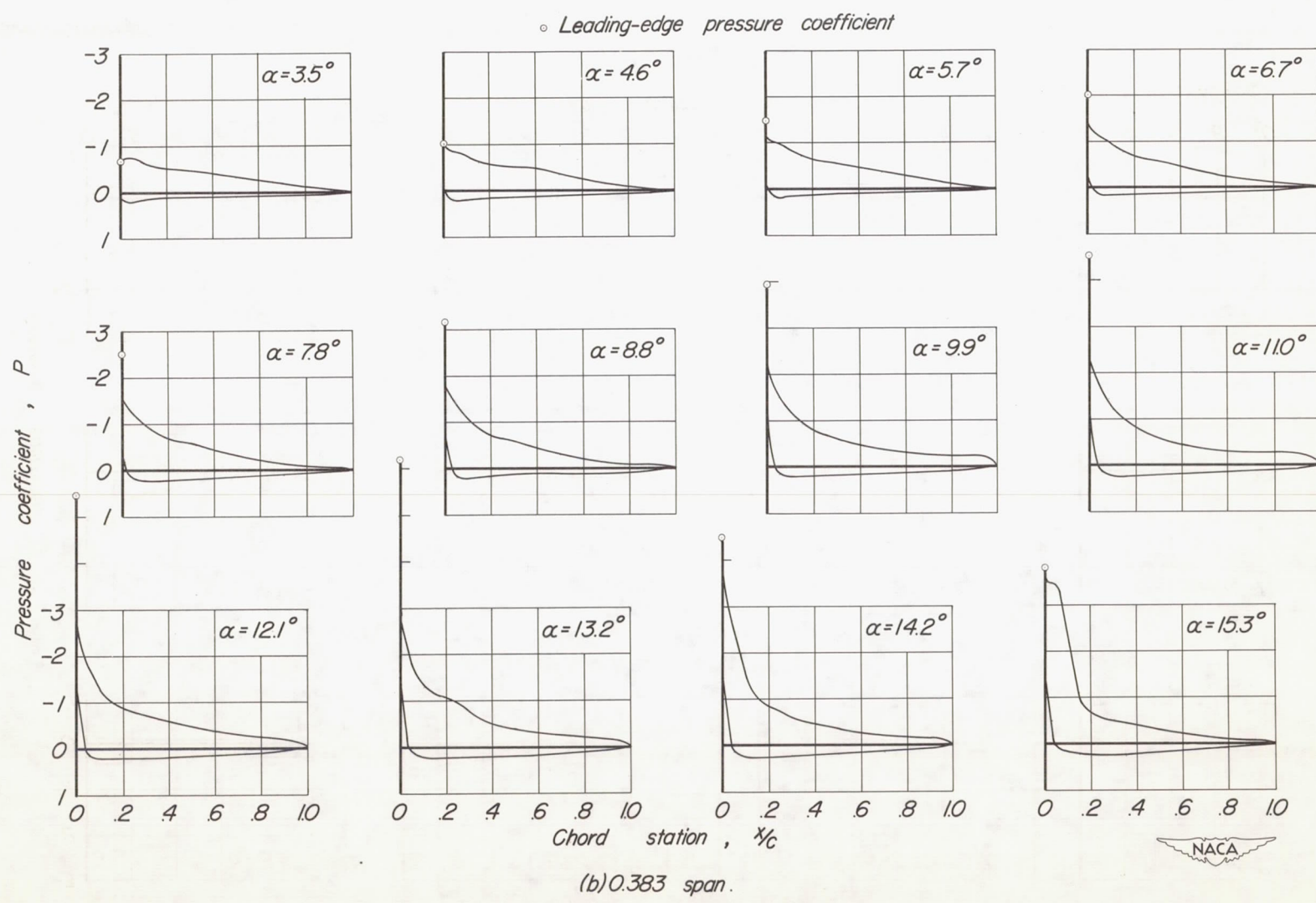


Figure 13-Continued.

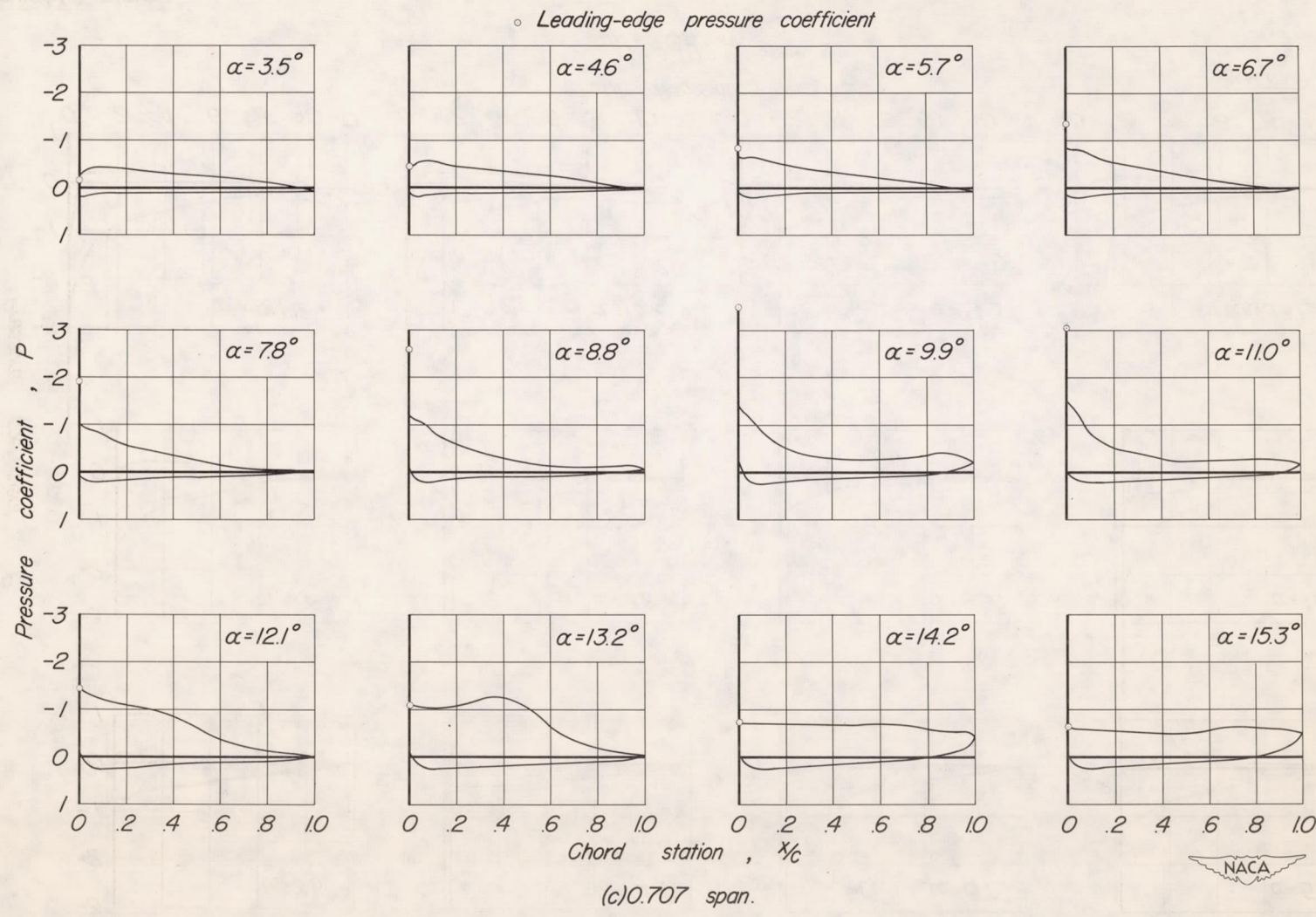


Figure 13:Continued.

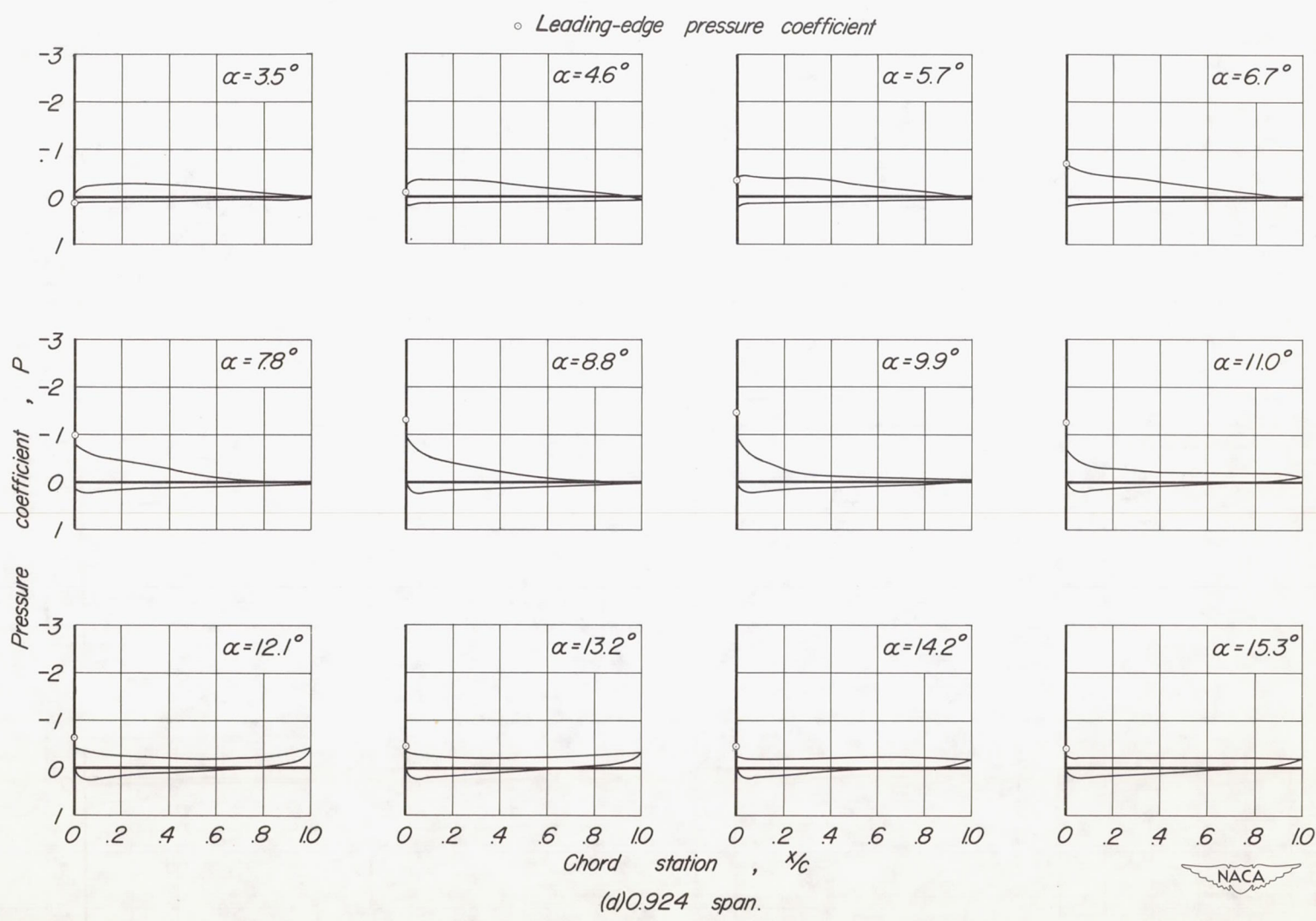


Figure 13.-Concluded.

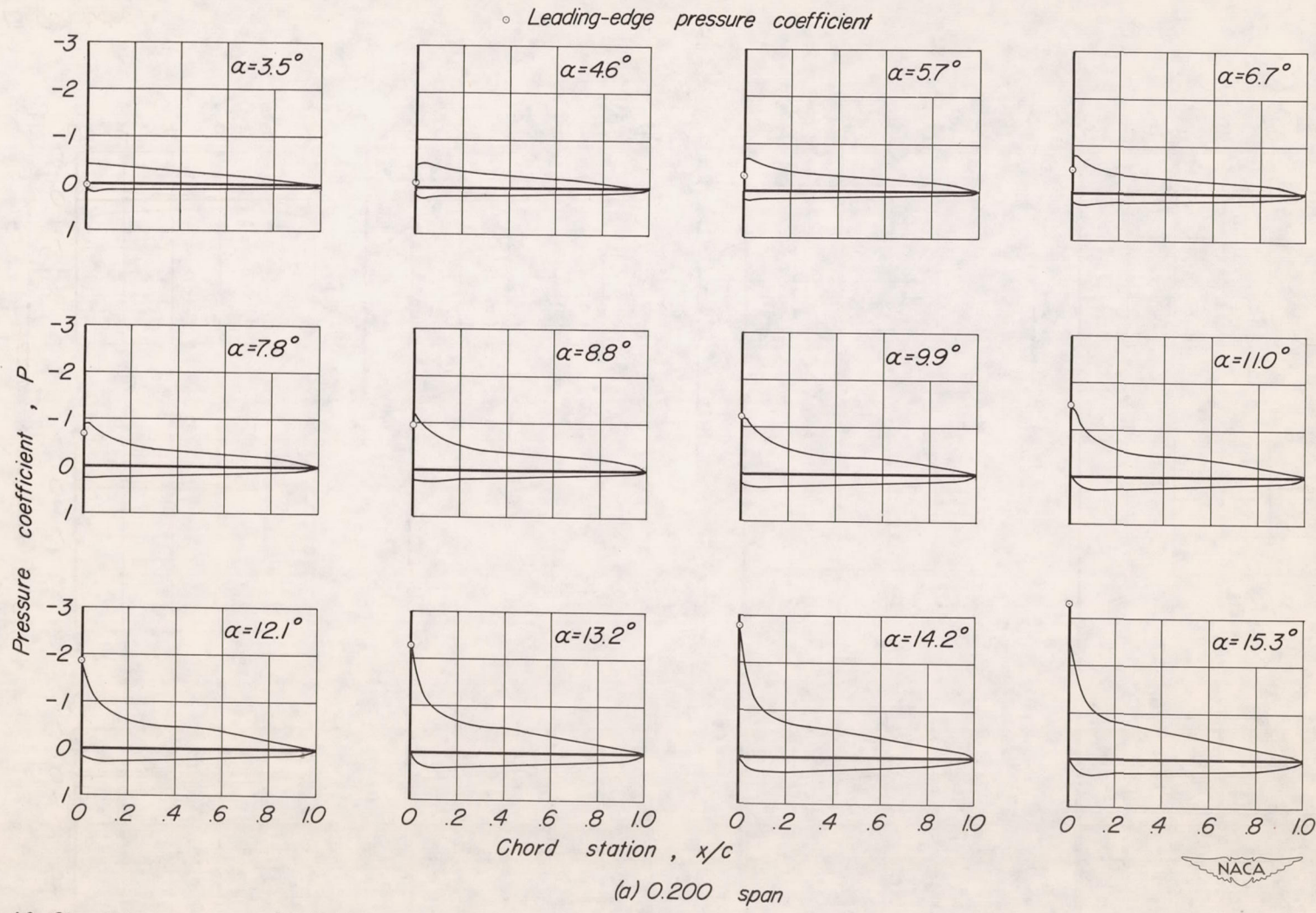


Figure 14.-Chordwise pressure distribution on the wing with fuselage.

○ Leading-edge pressure coefficient

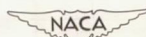
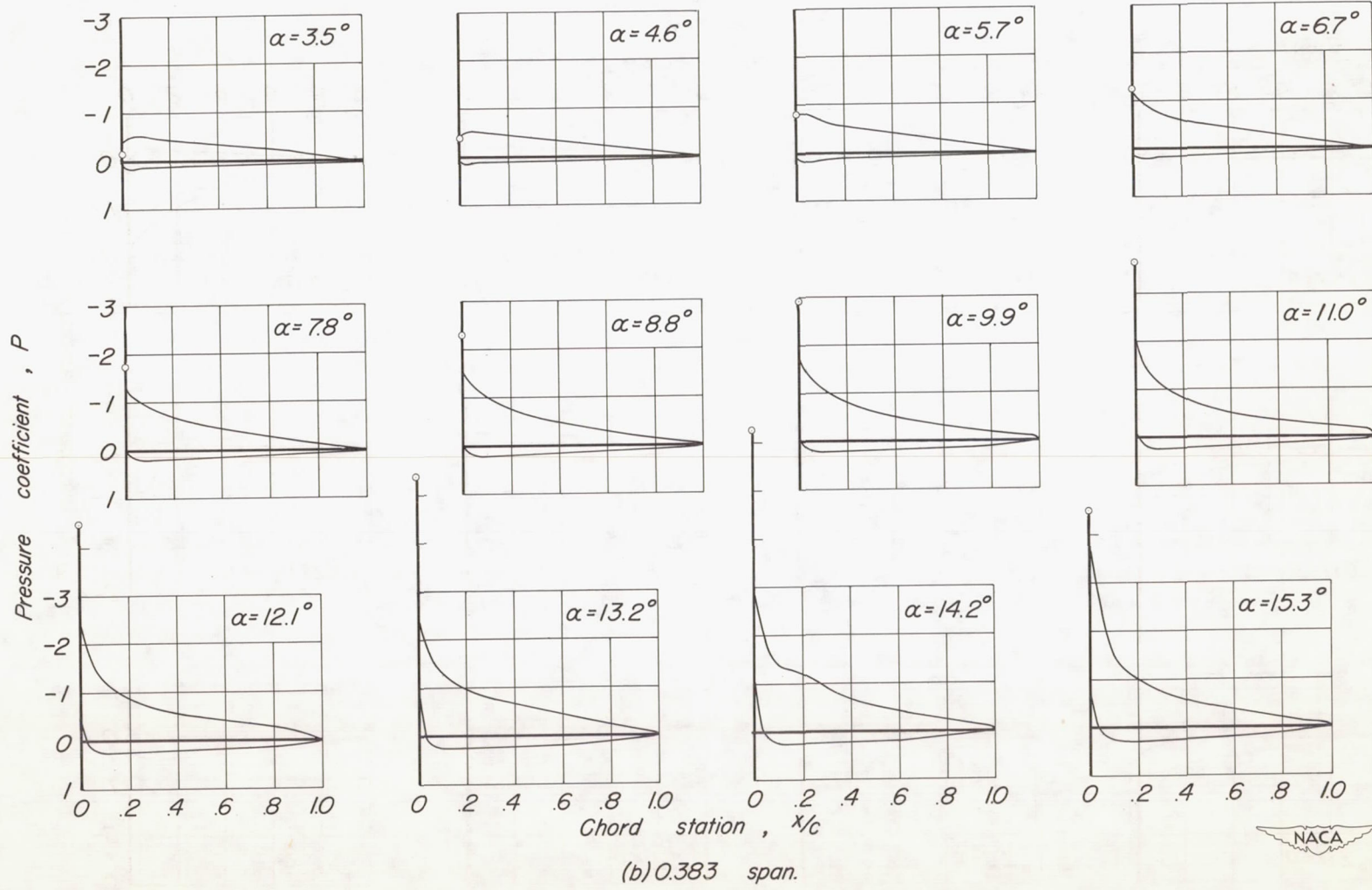


Figure 14.—Continued.

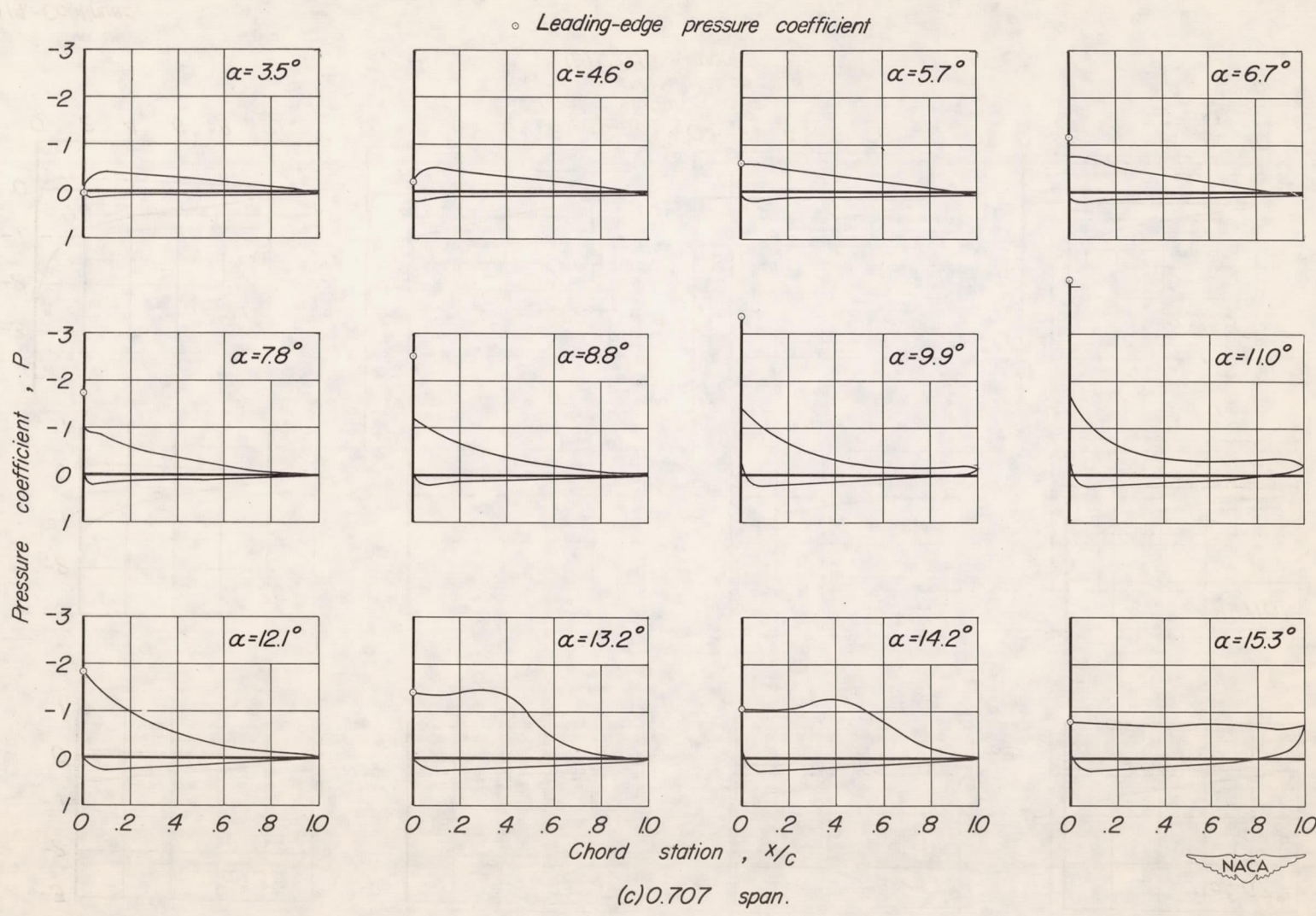


Figure 14.-Continued.

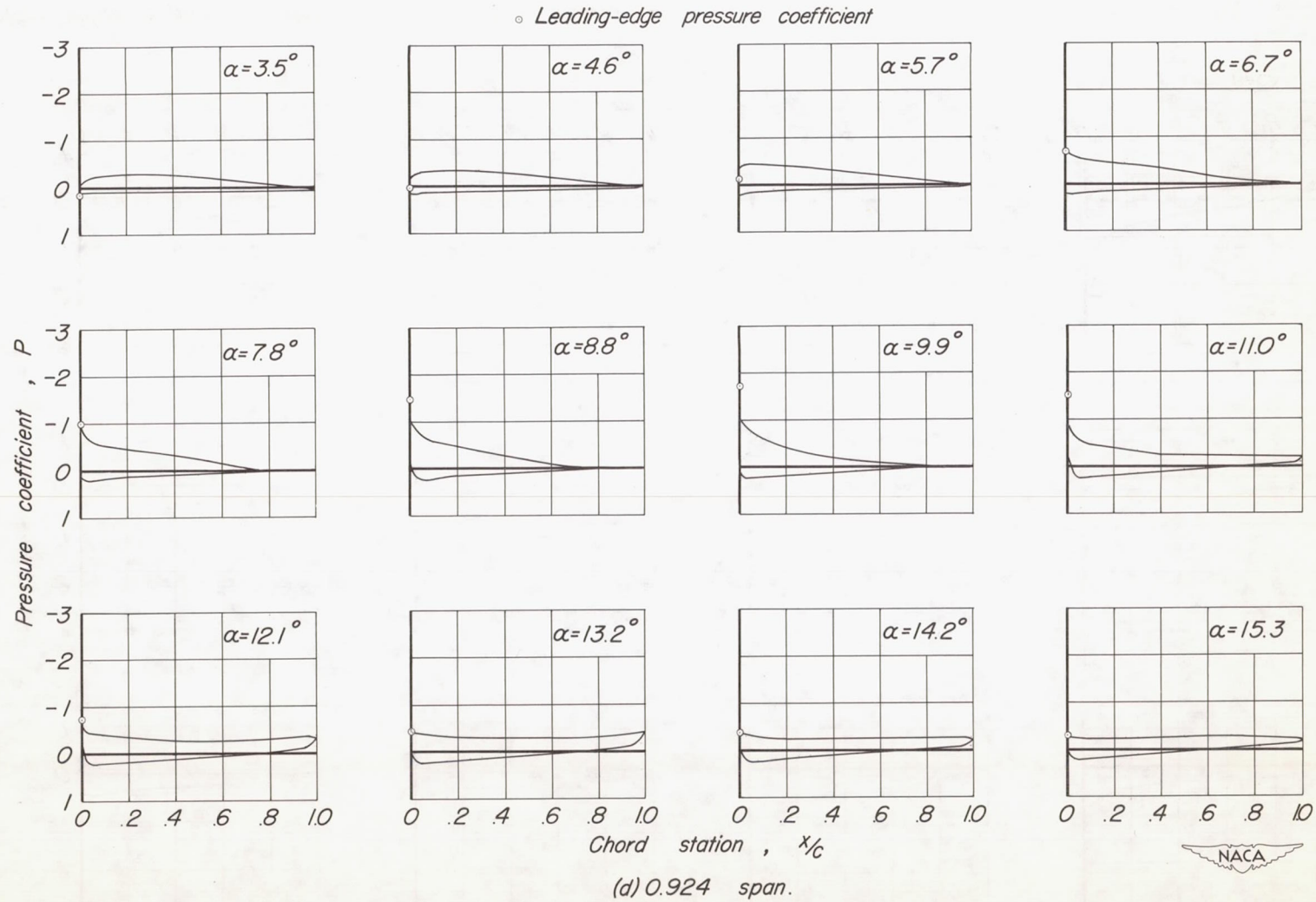


Figure 14.-Concluded.

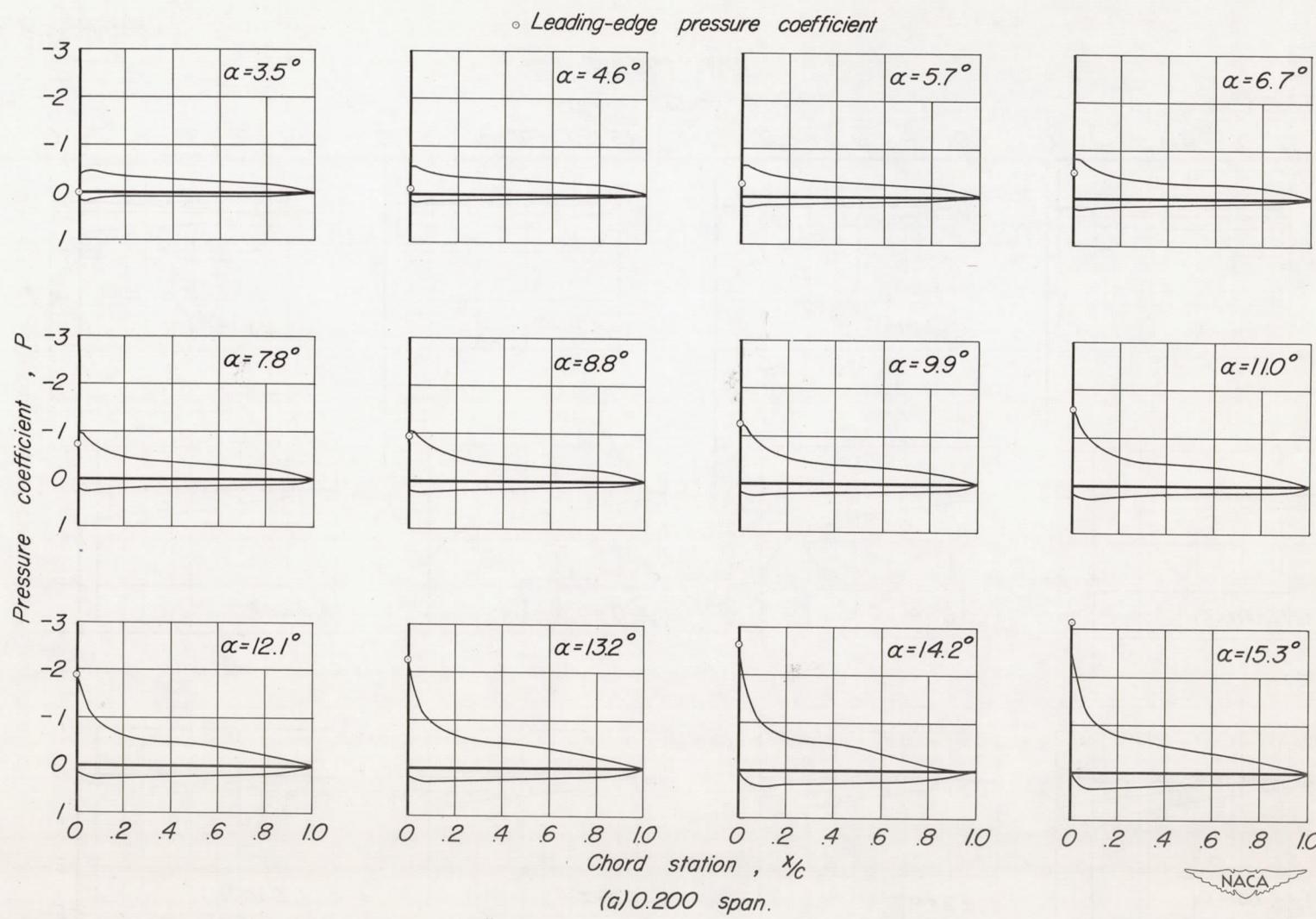


Figure 15.—Chordwise pressure distribution on the wing with fuselage and with fences at 0.6 and 0.8 span.

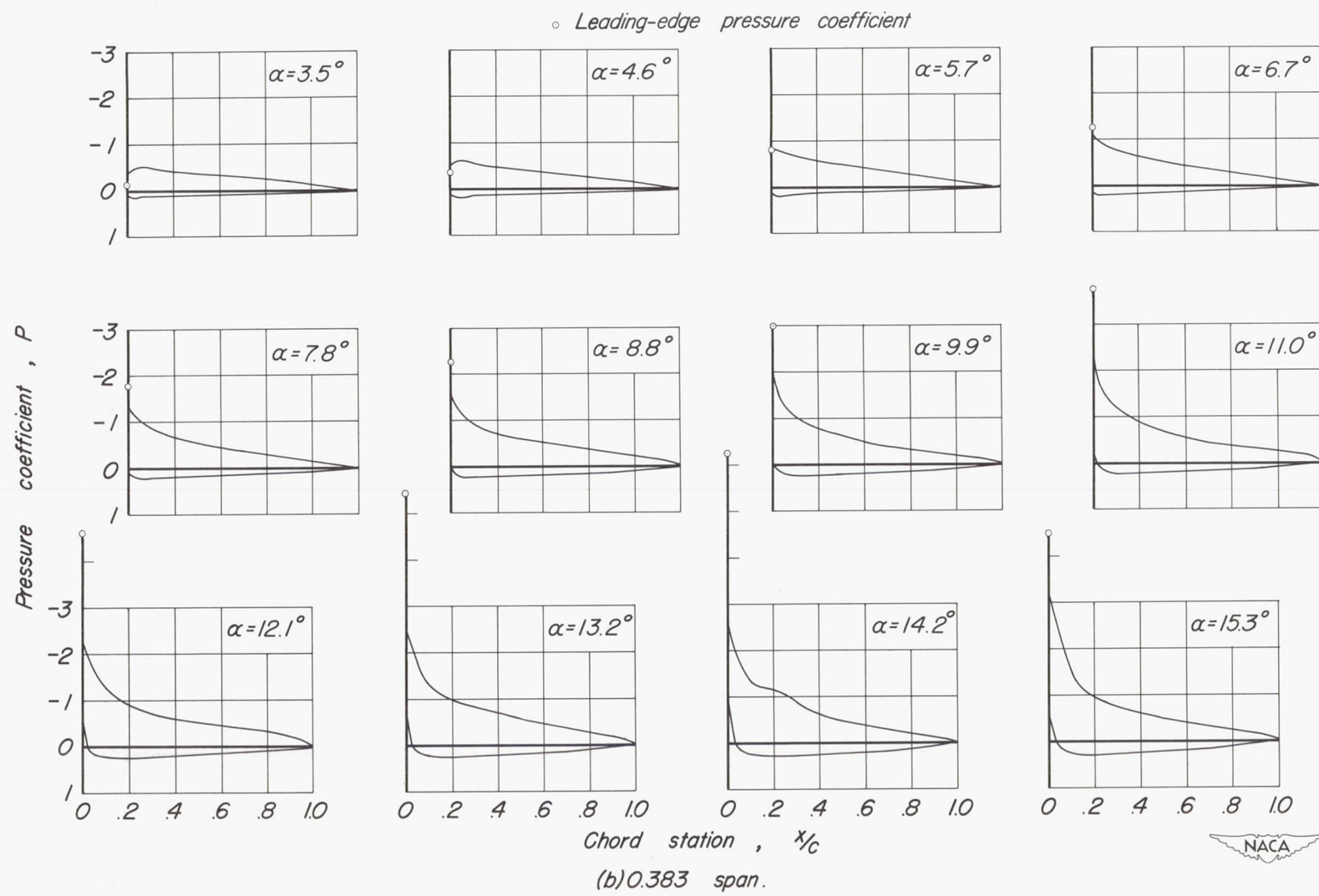


Figure 15—Continued.

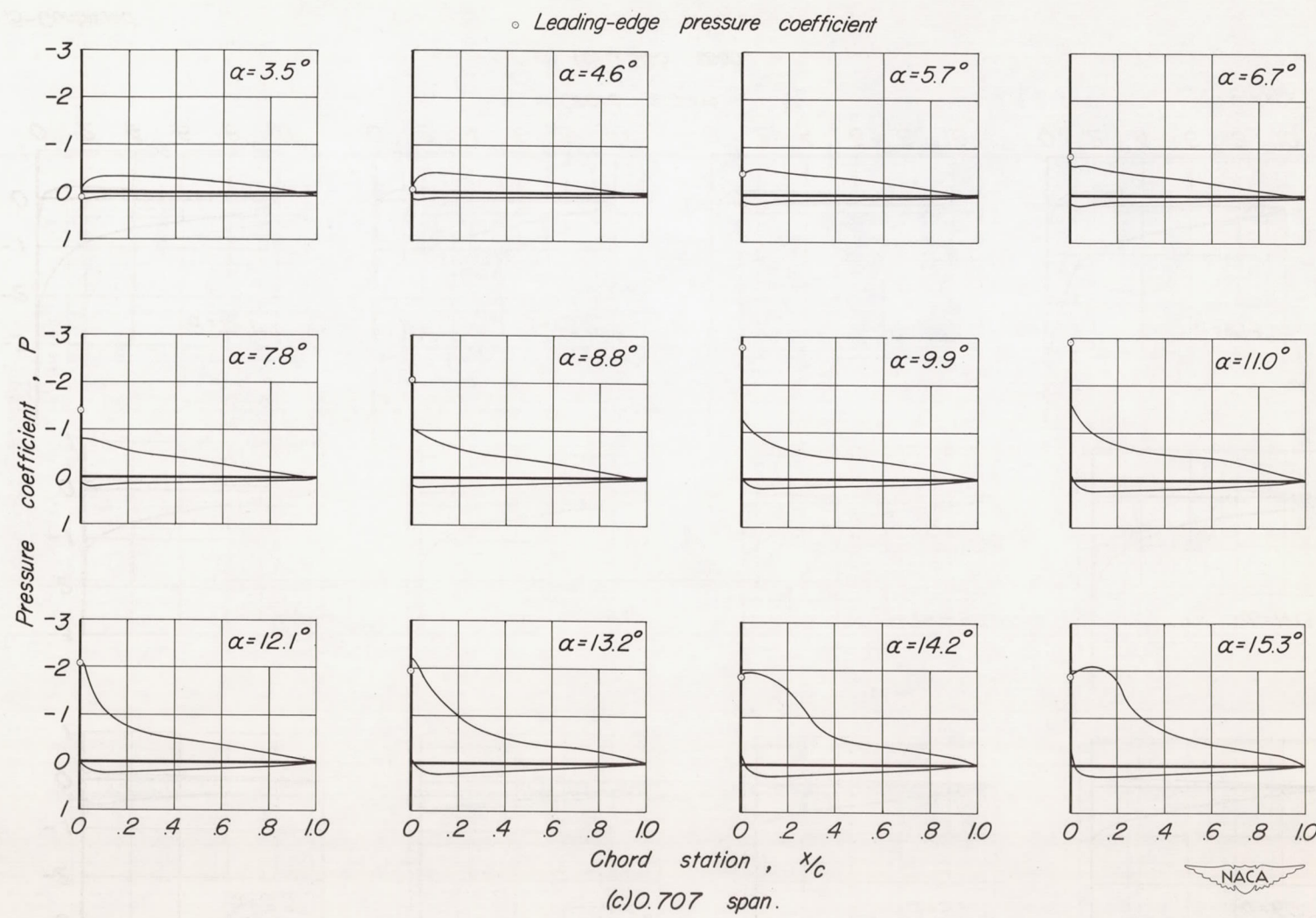


Figure 15-Continued.

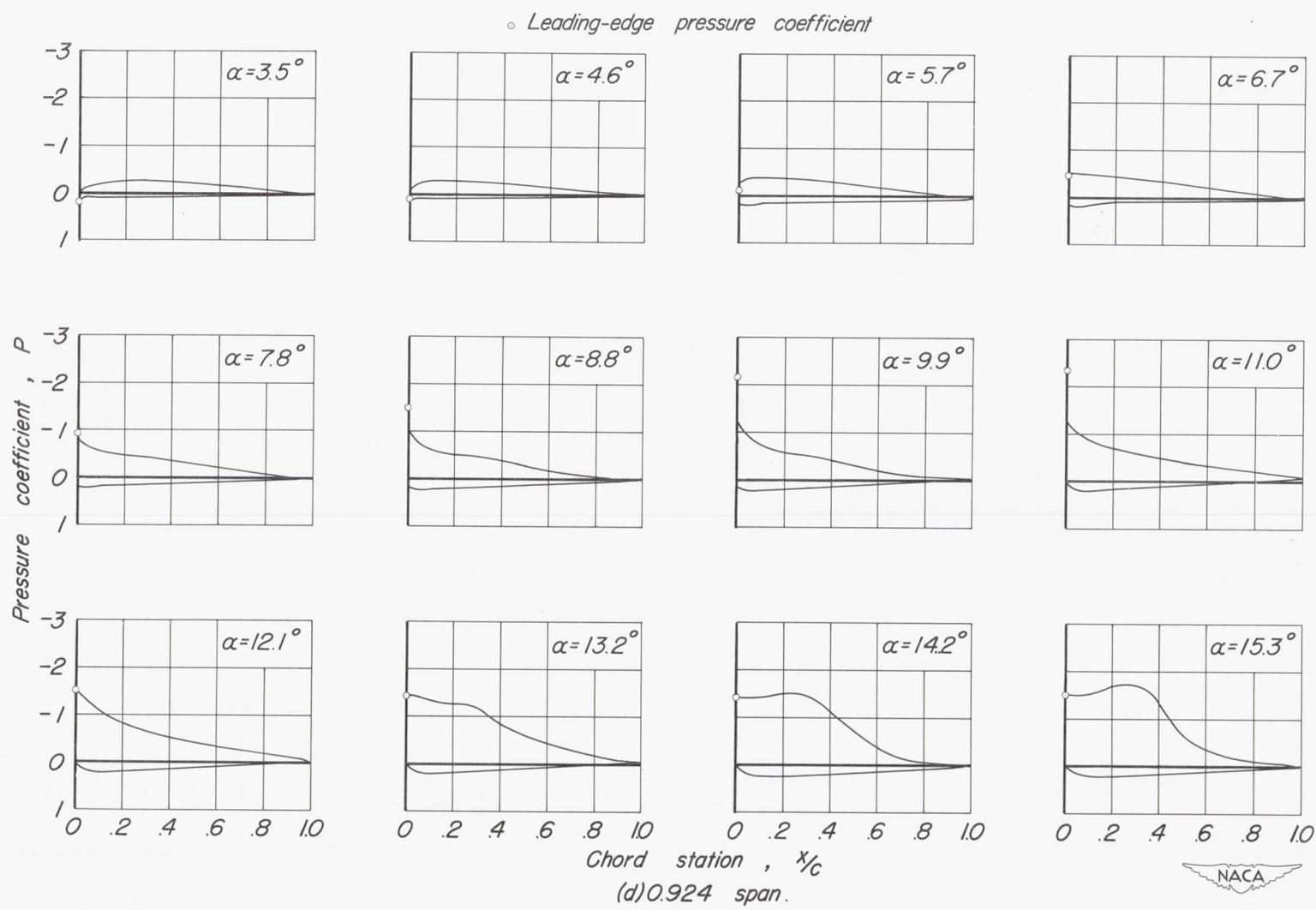
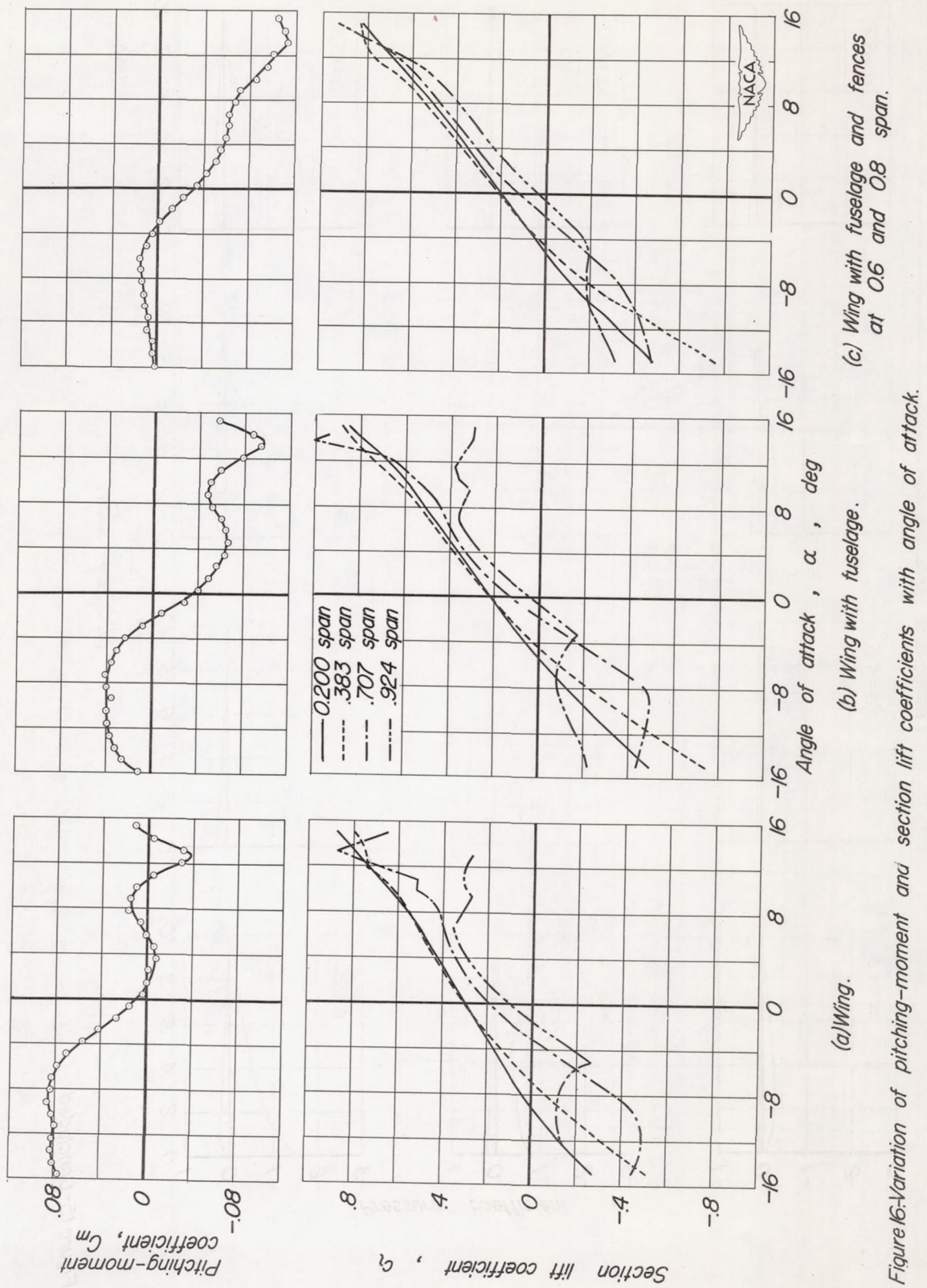
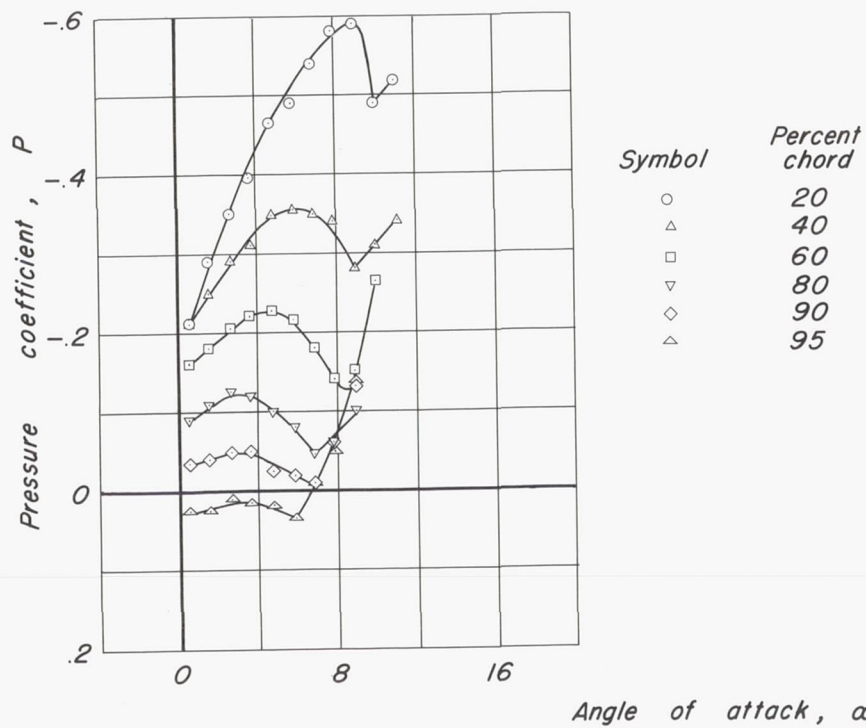
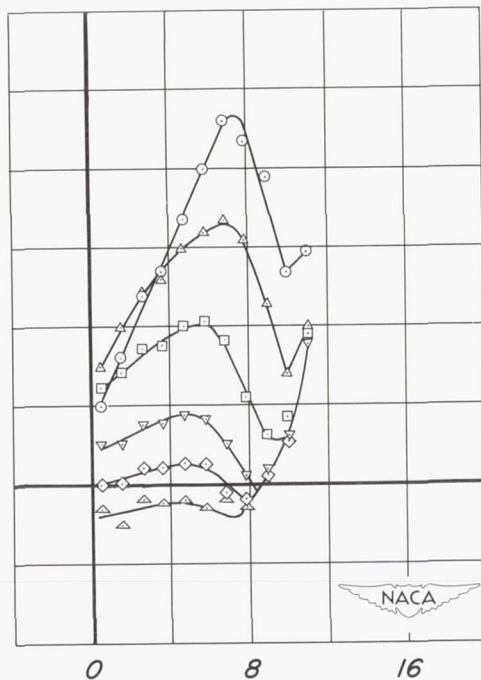


Figure 15-Concluded.



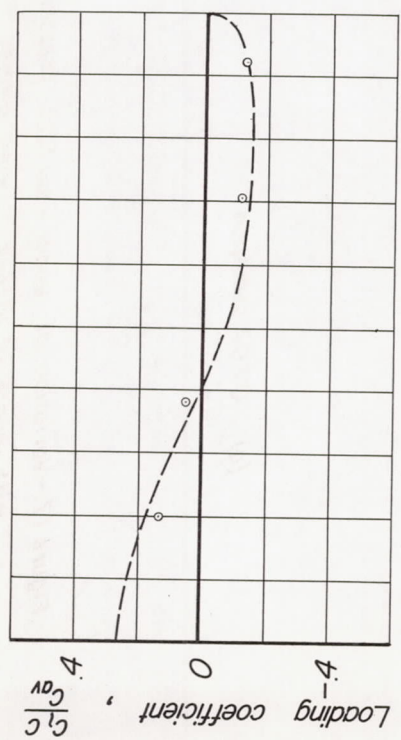


(a) 0.707 semispan.

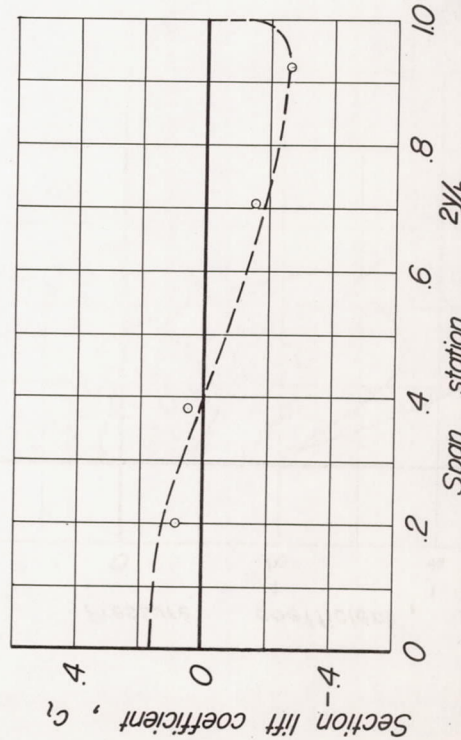


(b) 0.924 semispan.

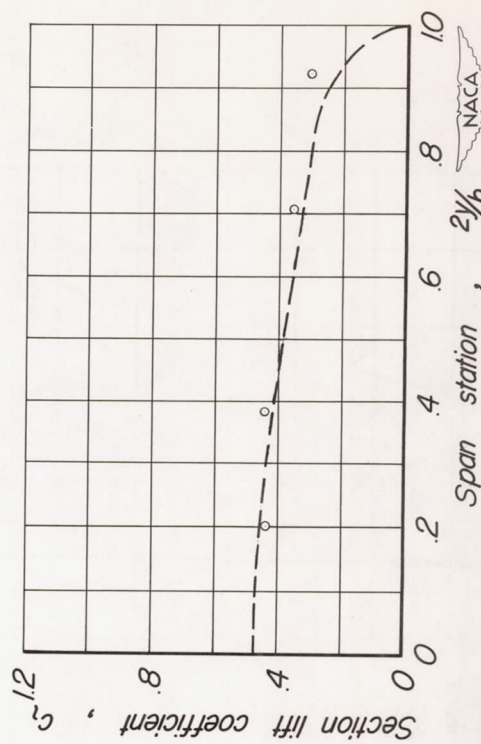
Figure 17—Variation of upper-surface pressure coefficient at several chordwise stations with angle of attack, wing alone.



— Theory  
○ Experiment



(a) Basic.



(b) Basic plus additional for  $C_L = 0.4$ .

Figure 18: Comparison of theoretical and experimental span loading for the wing.